Proceedings of the
Annual Stability Conference
Structural Stability Research Council
Louisville, Kentucky, April 13-16, 2021

Behavior, strength and DSM design of CFS lipped channel columns failing in global-global interactive modes

Elisa Cerqueira[1], Pedro B. Dinis[2], Dinar Camotim[2], Alexandre Landesmann[1], André D. Martins[2]

Abstract

This paper reports the latest results concerning an ongoing numerical investigation of the post-buckling behavior, strength and Direct Strength Method (DSM) design of cold-formed steel moderately long columns experiencing interaction between major-axis flexural-torsional (critical) and minor-axis flexural buckling – a coupling phenomenon involving two global buckling modes that was recently unveiled by Dinis *et al.* (2020a), in the context of fixed-ended plain channel (U) columns. These authors also (i) showed that the failure load erosion caused by this global-global (G-G) interaction cannot be captured by the currently available design methodologies and (ii) developed a DSM-based design approach able to handle cold-formed steel columns buckling in major-axis flexural-torsional modes that are either affected or unaffected by G-G interaction – this design approach provides efficient (safe, accurate and reliable) failure load predictions for fixed-ended U columns. The purpose of this work is to extend the scope of the previous study, by considering fixed-ended lipped channel (C) columns affected by different levels of G-G interaction, displaying various geometries (cross-section dimensions and lengths) and covering a wide slenderness range. After providing a brief overview of the DSM-based design approach proposed by Dinis *et al.* (2020a), the paper presents and discusses the new numerical results, involving almost exclusively C columns (but also a few U columns). These results concern the C column (i) buckling behavior, essential to select columns susceptible to G-G interaction, and (ii) elastic and elastic-plastic post-buckling behavior and strength – particular attention is paid to the identification of the most detrimental initial geometrical imperfection. Then, after assembling all the selected column failure load data, they are used to assess the quality of their predictions provided by the existing DSM-based design curves – it is found that the one proposed by Dinis *et al.* (2020a), in the context of U columns, can be readily applied, without any modifications, also to C column. This finding strengthens the belief that the methodology adopted will also be successful (possibly with slight modifications) for columns exhibiting other cross-section shapes and/or end support conditions – work is currently under way to confirm this belief.

1. Introduction and Background

Cold-formed steel members invariably display very slender thin-walled open cross-sections, a feature making them highly susceptible to several instability phenomena, namely local, distortional and global (flexural or flexural-torsional) buckling – Figs. 1(a)-(d) show lipped channel (C) column cross-sections

[1] Programa de Engenharia Civil, COPPE, Universidade Federal do Rio de Janeiro, Brazil. <elisa.cerqueira@coc.ufrj.br; alandes@coc.ufrj.br>

[2] CERIS, DECivil, Instituto Superior Técnico, Universidade de Lisboa, Portugal. <dinis@civil.ist.utl.pt; dcamotim@civil.ist.utl.pt; andrerdmartins@tecnico.ulisboa.pt>

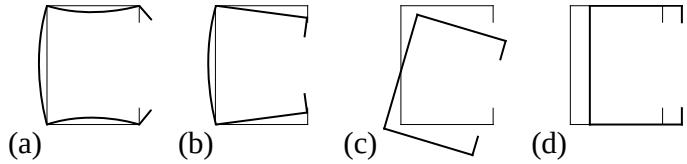

Figure 1: C column cross-sections buckled in (a) local, (b) distortional, (c) flexural-torsional and (d) flexural modes

buckled in local, distortional, flexural-torsional and flexural modes. Therefore, the ultimate strength and failure of such members are bound to be affected, to a larger or smaller extent, by the presence of one (pure failures) or more (interactive failures) of these instability phenomena – this explains why they must almost always be accounted for in cold-formed steel specifications (they can only be ignored in the design of stocky members, exhibiting "compact" cross-sections).

Nowadays, it can be rightfully argued that the Direct Strength Method (DSM – *e.g.*, Schafer 2008, 2019 or Camotim *et al.* 2016), first proposed by Schafer & Peköz (1998) and based on an original idea of Hancock *et al.* (1994), is the most rational and efficient approach for the design of cold-formed steel members (columns and beams, to be more precise) – this explains its fast growing and widespread popularity around the world. Moreover, it should be noted that the domain of application of the DSM has been recently extended to cover also beam-columns (Torabian & Schafer 2018), even if this research effort did not yet reach the codification stage. The currently codified design/strength curves are able to handle local, distortional, global and local-global interactive failures. In the context of this investigation, the relevant column nominal strength is the global one (P_{nG}), given by

$$P_{nG} = \begin{cases} P_y \left(0.658^{\lambda_G^2} \right) & if \quad \lambda_G \leq 1.5 \\ P_y \left(\dfrac{0.877}{\lambda_G^2} \right) & if \quad \lambda_G > 1.5 \end{cases} \qquad \text{with} \qquad \lambda_G = \sqrt{\frac{P_y}{P_{crG}}} \qquad (1)$$

where P_{crG} and λ_G are the column global critical buckling load and slenderness, and $P_y = A f_y$ is the column squash load (A and f_y are the cross-sectional area and steel yield stress, respectively). This design curve, combining an exponential expression (Ziemian 2010) with the (lowered) Euler curve, was first included in the North American cold-formed steel design specification in 1996 (AISI 1996), due to the work of Peköz & Sümer (1992), who showed that the above design curve, previously codified in the context of hot-rolled steel members used in buildings (AISC 1986), yielded a better failure load prediction quality than that adopted at that time by the cold-formed steel community (AISI 1986).

Recently, Dinis *et al.* (2019, 2020b) reported numerical studies on the accuracy of the current DSM column global strength curve in predicting the failure loads of fixed-ended cold-formed steel (CFS) columns collapsing in major-axis flexural-torsional (F_MT) or minor-axis flexural (F_m) modes – a wide parametric study was carried out to gather failure loads of columns with (i) several cross-sections (plain channels, unstiffened, return lip, web-stiffened and web/flange-stiffened lipped channels, lipped zed-sections, hat-sections, rack-sections and I-sections formed by back-to-back plain channels), (ii) various geometries (cross-section dimensions and lengths) and (iii) many slenderness values. While the column failure loads corresponding to F_m collapses are generally well predicted (there is only room for slight improvements in the low and intermediate slenderness ranges), it was shown that those associated with F_MT collapses are often considerably underestimated by the current design curve in the moderate and high slenderness ranges (Dinis *et al.* 2019). This fact led Dinis *et al.* (2020b) to propose a novel DSM-based strength curve set dependent on the non-dimensional cross-section geometric parameter

$$\beta_{FT} = \frac{I_I + I_w/A}{I_{II}} \tag{2}$$

where A, I_I, I_{II} and I_w are the cross-sectional area, major and minor moments of inertia, and warping constant (Dinis *et al.* 2020b). This strength curve set, termed P_{nFT}[3] and defined by

$$P_{nFT} = \begin{cases} P_y\left(0.658^{\lambda_{FT}^2}\right) & if \quad \lambda_{FT} \le 1.5 \\ P_y\left(\dfrac{a}{\lambda_{FT}^b}\right) & if \quad \lambda_{FT} > 1.5 \end{cases} \qquad \text{with} \qquad \lambda_{FT} = \sqrt{\frac{P_y}{P_{cr.FT}}} \tag{3}$$

where the β_{FT} dependence is felt through parameters a and b, obtained by means of a "trial-and-error curve fitting procedure", which read

$$a = 0.39 \times 1.5^b \qquad b = 0.06\beta_{FT} + 0.71 \le 2.0 \tag{4}$$

It should be noted that Eqs. (3) and (1) only differ for λ_{FT}>1.5 (moderate and high slenderness ranges) – the exponential expression is kept in the low-to-moderate slenderness range ($\lambda_{FT}\le$1.5). Each β_{FT} value leads to a and b values defining a different strength curve. For $\beta_{FT}\ge$21.5, one has b=2.0 and a=0.877, which means that Eq. (3) and (1) coincide. Figs. 2(a)-(b) plot, against λ_{FT} (=λ_G), the P_u/P_{nG} and P_u/P_{nFT} values concerning all numerical failure loads considered by Dinis *et al.* (2020b) – recall that the two plots only differ for λ_{FT}>1.5. Both figures include the P_u/P_{nG} and P_u/P_{nFT} means, standard deviations and maximum/minimum values, as well as the LRFD resistance factor ϕ values (AISI 2016) they lead to. It is clear that the proposed strength curve set yields accurate and mostly safe F_MT failure load predictions: the P_u/P_{nFT} mean and standard deviation are equal to 1.061-0.054 and lead to a LRFD resistance factor much higher than that prescribed by AISI (2016) for compression members (ϕ_c=0.85). Moreover, the large underestimations and scatter exhibited by the P_{nG} failure load estimates, for λ_{FT}>1.5, are eliminated.

Dinis *et al.* (2020b) also investigated CFS columns failing in F_MT modes and exhibiting other than fixed-ended support conditions (F columns), namely three types of pinned supports, all of them fixed with respect to torsion and having warping fully prevented: supports consisting of hinges that are either cylindrical (pinned with respect to major or minor-axis bending – PC_M and PC_m columns) or spherical

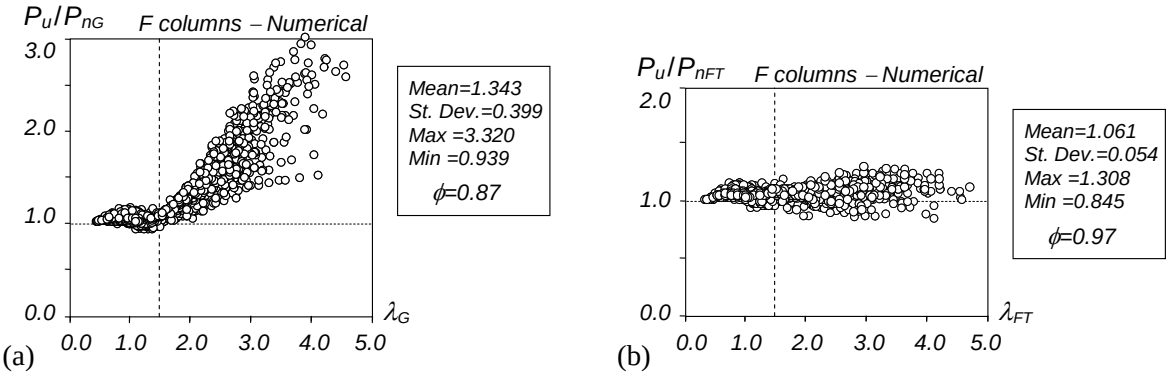

Figure 2: Plots (a) P_u/P_{nG} vs. λ_G and (b) P_u/P_{nFT} vs. λ_{FT} for the numerical F_MT failure loads considered by Dinis *et al.* (2020b)

[3] In order to make a clear distinction between the current DSM global design curve and the proposed DSM-based strength curve set, concerning exclusively columns failing in F_MT modes, subscript "G" was replaced by "FT" in the latter.

(pinned with respect to major and minor-axis bending – PS columns) – the investigation involved trios of identical PC_M, PC_m and PS columns with plain channel, lipped channel, return lipped channel, hat and rack cross-sections. In this context, it was found that the currently codified DSM column global design curve (P_{nG}) (i) predicts adequately (safely and accurately) the F_MT failure loads of the PS columns, along the whole slenderness range, (ii) underestimates the F_MT failure loads of the PC_M columns with λ_{FT}>1.5 (but by smaller amounts than their F counterparts) and (iii) overestimates the F_MT failure loads of the PC_m columns with λ_{FT}>1.0. In other words, it was concluded that the F_MT failure load prediction quality provided by the P_{nG} values varies considerably with the column end support conditions – this unexpected conclusion led the authors to further investigate this issue.

A close inspection of the columns analyzed revealed that there is a major difference between the F+PC_M and PC_m+PS column pairs: the ratios between the F_m (non-critical – $P_{b.Fm}$) and F_MT (critical – $P_{cr.FT}$) buckling loads are much smaller in the latter than in the former (*i.e.*, the ratio $P_{b.Fm}/P_{cr.FT}$ is closer to 1.0). Moreover, it was also found that it is virtually impossible to select PC_m or PS column geometries that preclude the closeness between $P_{b.Fm}$ and $P_{cr.FT}$ ($P_{b.Fm}/P_{cr.FT}$ is never far from 1.0) – unlike in F or PC_M columns, for which an appropriate geometry selection enables a fine "control" of $P_{b.Fm}/P_{cr.FT}$ (it can be either much higher, moderately higher or close to 1.0). This finding raised the suspicion and subsequently convinced the authors that the column F_MT post-buckling behavior and strength is influenced by the coupling between F_MT and F_m buckling – the closeness of $P_{b.Fm}/P_{cr.FT}$ to 1.0 quantifies the relevance of this interaction phenomenon. Note that, to the authors' best knowledge, a global-global (G-G) interaction had only been unveiled in short-to-intermediate equal-leg angle columns (*e.g.*, Camotim *et al.* 2020), due to their very specific and peculiar geometry (formed by just two outstand walls). On the other hand, the type of G-G interaction addressed in this work is bound to occur in columns with singly symmetric cross-sections (symmetry with respect to the major-axis) that buckle in F_MT critical modes.

In view of the content of the previous paragraph, it can be logically argued that (i) PC_m and PS columns are invariably affected by F_MT-F_m (global-global) interaction, while (ii) the F and PC_M columns may be affected by this coupling phenomenon or not, depending on the closeness of $P_{b.Fm}/P_{cr.FT}$ to 1.0. Therefore, in order to assess the relevance of global-global interaction in eroding the column F_MT failure loads, Dinis *et al.* (2020b) decided to compare the failure loads of two sets of CFS fixed-ended U columns sharing the same cross-section dimensions (b_w=100 mm, b_f=40 mm, t=1.2 mm), yield stresses and initial geometrical imperfections (critical-mode F_MT imperfections with amplitude L/1000). Only columns such that λ_{FT}>1.5 were considered, since the interaction effects are always stronger in slender columns. Fig. 3(a) displays the plots P_u/P_{nFT} vs λ_{FT} for the two sets of fixed-ended U columns – the white and grey circles stand, respectively, for columns with R_G= $P_{b.Fm}/P_{cr.FT}$ values either above or below 1.45 – this quite arbitrary "border" aimed at separating U columns unlikely or likely to be affected by F_MT-F_m interaction. It became clear that, as expected, the white P_u/P_{nFT} values were consistently well above their grey counterparts, evidencing the failure load erosion caused by the G-G interaction. In addition, it was also observed that the P_{nFT} estimation of the second (grey) failure load set is clearly inadequate (inaccurate and unsafe) – indeed, almost all P_u/P_{nFT} values are below 1.0 (many of them substantially). Conversely, the same estimation of the first (white) failure load set is very good – not surprising, since the development and validation of the P_{nFT} DSM-based design approach was based, almost solely, on failure loads of columns with R_G values much higher than 1.0 (Dinis *et al.* 2020b). The corresponding statistical indicators (mean, standard deviation and maximum/minimum values) made it possible to quantify the difference in failure load prediction quality: 0.74-0.14-1.01-0.50 (grey circles) vs. 1.08-0.08-1.21-0.85 and show the inadequacy of the P_{nFT} values in predicting failure loads of U columns affected by G-G interaction. This finding prompted the research effort whose fruits were reported by Dinis *et al.* (2020a).

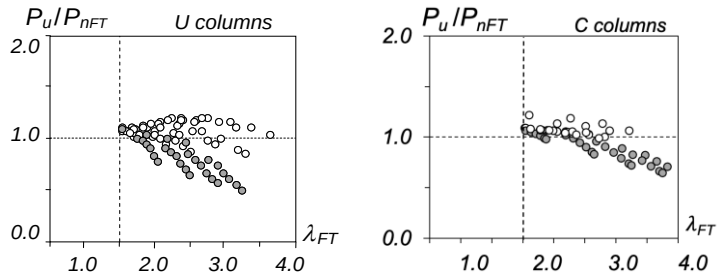

Figure 3: Plots P_u/P_{nFT} vs. λ_{FT} for (a) U and (b) C columns with $P_{b.Fm}/P_{cr.FT}$ above (white circles) and below (grey circles) 1.45

They included a modification of the column strength curve set proposed by Dinis *et al.* (2020b), which consisted of incorporating the buckling load ratio R_G in the expressions providing the strength curves, thus accounting for the F_MT-F_m interaction level. This modified/improved DSM-based design approach was shown to provide efficient (safe, accurate and reliable) failure loads for fixed-ended U columns buckling in F_MT modes, regardless of their R_G value (*i.e.*, whether they are affected or not by F_MT-F_m interaction).

The purpose of this work is to extend the study reported by Dinis *et al.* (2020a) to CFS lipped channel (C) columns, *i.e.*, to investigate whether and to which extent F_MT-F_m interaction affects their behavior, strength and DSM-based design – naturally, it seems fair to expect that the outcome of this investigation will be similar (at least qualitatively) to that obtained for U columns. This expectation is strengthened by the plots P_u/P_{nFT} vs λ_{FT} displayed in Fig. 3(b), similar to their Fig. 3(a) counterparts. They concern fixed-ended C columns (b_w=95mm, b_f=50mm, b_l=10 mm, t=1.8 mm) buckling in F_MT modes and with R_G either above or below 1.45, and their P_u/P_{nFT} statistical indicators are close to the U column ones (0.86-0.13-1.06-0.64 and 1.07-0.05-1.21-0.99, respectively for the grey and white circles), which confirms that the P_{nFT} values are also inadequate to predict failure loads of C columns affected by G-G (F_MT-F_m) interaction.

After presenting an overview of the DSM-based design approach developed for U columns affected by G-G interaction (Dinis *et al.* 2020a), the paper addresses the C column buckling behavior and the selection of column geometries prone to various levels of G-G interaction. Then, the elastic and elastic-plastic post-buckling behavior and strength of fixed-ended C columns affected by F_MT-F_m interaction are studied, adopting the same approach followed previously for the U columns. Next, the paper presents the results of a parametric study carried out to gather F_MT failure loads of C columns with (i) the various geometries selected earlier and (ii) several yield stresses, chosen to enable covering a wide slenderness range. Then, the assembled numerical F_MT failure load data are used to show that the DSM-based strength curve set proposed by Dinis *et al.* (2020a) can also be successfully adopted to handle G-G interactive failures of C columns buckling in F_MT modes. It predicts efficiently the failure loads of fixed-ended U and C columns buckling in F_MT modes, regardless of whether they are affected or not by G-G interaction – in addition, the high failure load prediction quality for columns unaffected by this interaction is retained. The findings reported by Dinis *et al.* (2020a) and in this paper encourage extending the adopted methodology to columns with other cross-section shapes and/or support conditions, thus paving the way for a general and unified DSM-based design method for CFS columns failing in F_MT (pure) or F_MT-F_m (interactive) modes.

2. Overview of the DSM-Based Design Approach Developed for U Columns (Dinis *et al.* 2020a)

On the sole basis of the failure loads obtained for fixed-ended U columns buckling in F_MT modes and either unaffected (large R_G values) of affected (R_G values close to 1.0) by G-G (F_MT-F_m) interaction, Dinis *et al.*

(2020a) showed that their failure loads can be adequately predicted by the strength curve set, termed $P_{nFT\text{-}G}$ and defined by the expressions

$$P_{nFT-G} = \begin{cases} P_y \left(0.658^{\lambda_{FT}^2}\right) & \text{if} \quad \lambda_{FT} \le 1.5 \\ P_y \left(\dfrac{a}{\lambda_{FT}^b}\right) & \text{if} \quad \lambda_{FT} > 1.5 \end{cases} \qquad \text{with} \qquad \lambda_{FT} = \sqrt{\frac{P_y}{P_{cr.FT}}} \tag{5}$$

$$a = 0.39 \times 1.5^b \tag{6}$$

$$b = 0.06\beta_{FT} + c \le 2.0 \tag{7}$$

$$c = -19.5\ R_G^3 + 73.6\ R_G^2 - 94.1\ R_G + 42\ \ge\ 0.71 \tag{8}$$

where β_{FT} is still given by Eq. (2). Note these expressions are a modification of Eqs. (3)-(4) – the difference is the fact that the strength curve set depends not only on β_{FT}, but also on R_G, via a new additive parameter c. Moreover, note also that Eqs. (3)-(4) are recovered for $R_G \ge 1.49$ (one has then $c=0.71$), which means that the fixed-ended U column failure load prediction quality achieved by Dinis *et al.* (2020b) remains unaltered. Figs. 4(a)-(b) make it possible to assess the performance and merits of the strength curve set proposed by Dinis *et al.* (2020a). They display plots $P_u/P_{nFT\text{-}G}$ vs. λ_{FT} concerning the U columns (i) reported by Dinis *et al.* (2020a), almost all affected by G-G interaction, and (ii) reported by Dinis *et al.* (2020b), whose R_G values are all much higher than 1.0 ($R_G \ge 1.45$) – both figures include the $P_u/P_{nFT\text{-}G}$ averages, standard deviations and maximum/minimum values. Moreover, Table 1 gives, for the two fixed-ended U column sets, the failure load numbers (n) and $P_u/P_{nFT\text{-}G}$ statistical indicators, separating the columns with $\lambda_{FT} \le 1.5$ and $\lambda_{FT} > 1.5$. It is clear that the proposed DSM-based column strength curve set, dependent on β_{FT} and R_G, provides high-quality failure load predictions for all the U columns analyzed by Dinis *et al.* (2020a,b), regardless of whether they are unaffected or affected by G-G interaction.

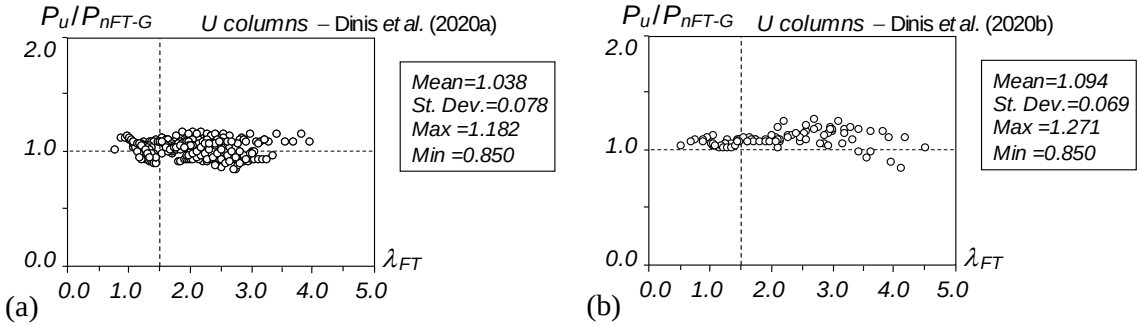

Figure 4: Plots $P_u/P_{nFT\text{-}G}$ vs. λ_{FT} for the U columns reported by (a) Dinis *et al.* (2020a) and (b) Dinis *et al.* (2020b)

Table 1: Statistical indicators of the $P_u/P_{nFT\text{-}G}$ values concerning the fixed-ended U columns reported by Dinis *et al.* (2020a,b)

U Columns	Dinis *et al.* (2020a)		Dinis *et al.* (2020b)		All columns	
λ_{FT}	≤ 1.5	> 1.5	≤ 1.5	> 1.5	≤ 1.5	> 1.5
n	51	184	29	61	80	245
Mean	1.033	1.034	1.056	1.108	1.044	1.053
Sd. Dev.	0.069	0.078	0.028	0.078	0.059	0.084
Max	1.139	1.182	1.125	1.271	1.139	1.271
Min	0.905	0.850	1.017	0.850	0.905	0.850

3. Column Geometry Selection – Buckling Behavior

The signature curves depicted in Fig. 5(a) concern steel (E=210 GPa, ν=0.3) C columns with b_w=100 mm, b_f=60 mm, b_l=10 mm and four thickness values, namely t=2;3;4;5 mm. Each solid curve, providing the variation of the critical buckling stress f_{cr} with the length L (logarithmic scale), was obtained by means of GBT buckling analyses performed in the program GBTUL (Bebiano *et al*. 2018) and including the following 13 deformation modes: 4 global (**1-4**), 2 distortional (**5-6**) and 7 local (**7-13**). The dashed curve provides the variation of the minor-axis flexural buckling stress $f_{b.Fm}$ with L – this curve is the same for the 4 cross-section geometries. Fig. 5(b) shows the GBT modal participation diagrams associated with each f_{cr} vs. L curve, providing the contributions of each GBT deformation mode to the column buckling modes (*e.g.*, a t=3mm column with L=500 cm buckles in a mode combining participations from modes **2** and **4** – 11.7% and 88.3%, respectively). Finally, Fig. 5(c) shows the in-plane shapes of the GBT deformation modes **2-5** and the critical buckling modes of t=3mm C columns with L=150, 600, 1200 cm. These buckling results prompt the following remarks:

(i) Each f_{cr} vs. L curve exhibits two distinct zones, one associated with distortional buckling in modes with various half-waves (only p_5 exists and f_{cr} remains practically constant) and the other with single half-wave global buckling. In the latter zone, f_{cr} decreases monotonically with L and the columns buckle in either F_MT (**2**+**4**) modes with dominant torsional deformation or F_m (**3**) modes –the change in buckling mode nature occurs abruptly, at the "transition length" L=L_T.

(ii) Because the column F_m buckling stress is virtually independent of t, the 4 F_MT signature curve branches, each concerning columns with a different t value, end in a common F_m signature curve branch – see Fig. 5(a).

(iii) Columns with L=L_T have coincident F_MT and F_m buckling stresses, which means that their post-buckling behaviors, strengths and failure stresses are bound to be affected by the interaction between

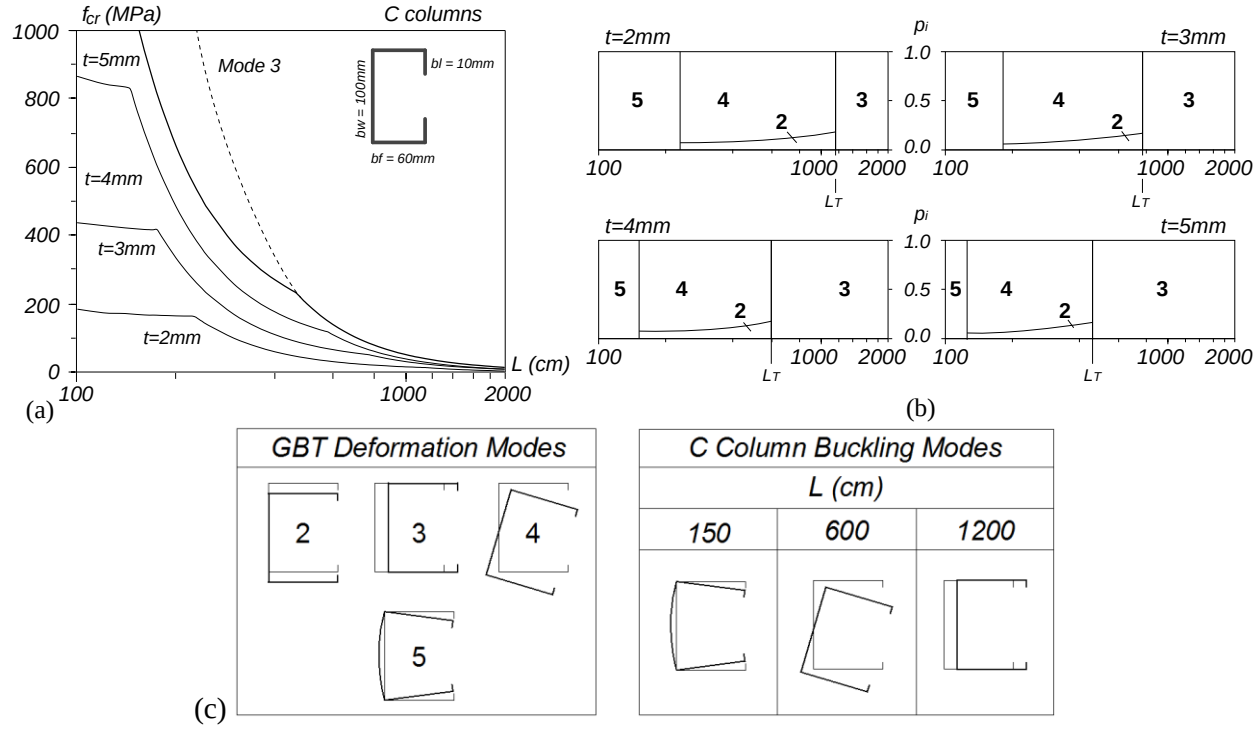

Figure 5: (a) f_{cr} vs. L curves and (b) GBT modal participation diagrams of C columns (b_w=100mm; b_f=60mm; b_l=10mm; t=2; 3; 4; 5mm), and (c) in-plane shapes of GBT deformation modes **2-5** and 3 critical buckling modes of t=3mm C columns

these two buckling modes (G-G interaction). However, it is expected that the interaction effects will also influence the post-buckling behavior, strength and failure load/stress of columns with lengths not too much smaller than L_T, *i.e.*, such that $P_{b.Fm}/P_{cr.FT}$ ($\equiv f_{b.Fm}/f_{cr}$) is not significantly higher than 1.0.

It is now necessary to identify column geometries associated with several levels of closeness between the column f_{cr} and $f_{b.Fm}$ buckling stresses. This is done by selecting columns with lengths lower than L_T (see Fig. 5(b)) – an upper limit $L = 850$ cm was defined to ensure that no column selected is unrealistically long. The 48 column geometries (b_w, b_f, b_l, t, L) selected ensure buckling in F_MT and $f_{b.Fm}/f_{cr}$ ratios comprised between 1.96 and 1.01. Table 2 provides the selected column cross-section dimensions and properties (b_w, b_f, b_l, t, A, b_w/b_f, I_I, I_{II}, I_w and β_{FT}), lengths (L_i), and buckling stresses and ratios (f_{cr}, $f_{b.Fm}$ and

Table 2: Selected C column geometries: b_w, b_f, b_l, t, A, I_I, I_{II}, I_w, L, $f_{cr.FT}$, $f_{b.Fm}$ and R_G values (mm, mm^2, mm^4, mm^6 and MPa)

Column	b_w	b_f	b_l	t	A	b_w/b_f	I_1	I_2	I_ω	β_{FT}	L		$f_{cr.FT}$	$f_{b.Fm}$	R_G
C1	60	55	11	4.5	8.6	1.09	52.2	33.7	305.4	2.60	L1	4800	157.80	136.34	1.37
											L2	5000	145.50	125.71	1.32
											L3	5500	120.20	103.85	1.22
											L4	6000	101.00	87.26	1.13
											L5	6500	86.10	74.39	1.06
											L6	7000	74.20	64.11	1.01
C2	100	60	10	3	7.2	1.67	127.2	36.0	724.4	6.32	L1	3500	337.90	243.29	1.84
											L2	4500	204.80	147.46	1.59
											L3	5500	137.10	98.71	1.37
											L4	6000	115.20	82.94	1.28
											L5	7000	84.70	60.98	1.11
											L6	7500	73.80	53.14	1.03
C3	120	80	15	5	15.5	1.50	401.8	141.9	4373.2	4.82	L1	4500	374.50	580.48	1.87
											L2	5500	250.90	388.90	1.62
											L3	6500	179.70	278.54	1.41
											L4	7500	135.00	209.25	1.23
											L5	8000	118.30	183.37	1.15
											L6	8500	105.10	162.91	1.08
C4	140	70	10	3.5	10.5	2.00	349.8	68.1	2529.9	8.68	L1	3400	459.50	482.48	1.58
											L2	4000	334.30	351.02	1.50
											L3	4500	264.80	278.04	1.43
											L4	5500	177.60	186.48	1.28
											L5	6500	127.20	133.56	1.14
											L6	7500	95.60	100.38	1.02
C5	80	65	15	5	12.0	1.23	127.4	68.0	1114.1	3.24	L1	5300	186.00	223.2	1.44
											L2	5500	172.70	207.2	1.39
											L3	6000	145.10	174.12	1.28
											L4	6500	123.70	148.44	1.18
											L5	7000	106.60	127.92	1.10
											L6	7600	90.40	108.48	1.03
C6	95	50	10	2	4.3	1.90	66.7	15.3	281.8	8.65	L1	2700	398.60	171.40	1.75
											L2	3500	239.50	102.99	1.63
											L3	4500	145.30	62.48	1.46
											L4	5500	97.30	41.84	1.30
											L5	6500	69.70	29.97	1.15
											L6	7500	52.40	22.53	1.02
C7	75	60	10	4	8.6	1.25	78.9	38.1	468.1	3.50	L1	5200	155.40	133.64	1.42
											L2	5500	138.90	119.45	1.34
											L3	6000	116.80	100.45	1.23
											L4	6500	99.50	85.57	1.13
											L5	6800	90.10	77.49	1.07
											L6	7200	81.10	69.75	1.02
C8	80	45	11	2	3.8	1.78	42.6	11.6	165.1	7.38	L1	2000	626.20	240.46	1.96
											L2	2500	397.10	152.49	1.83
											L3	3500	204.10	78.37	1.62
											L4	4500	123.60	47.46	1.40
											L5	5500	87.80	33.72	1.28
											L6	6500	59.30	22.77	1.04

$f_{b.Fm}/f_{cr} \equiv R_G$). It is worth noting that (i) there are 8 cross-section geometries whose dimensions are such that $2.00 \geq b_w/b_f \geq 1.09$ and $8.68 \geq \beta_{FT} \geq 2.70$, and (ii) the lengths are such that $8500 \geq L \geq 2000$ mm – all 8 cross-section geometries selected are combined with 6 lengths, thus enabling a variation of the R_G value.

4. Post-Buckling Behavior under Global-Global Mode Interaction – Imperfection-Sensitivity Study

A very important issue in mode interaction studies is to assess how the initial geometrical imperfection shape influences the post-buckling behavior and strength of the structural system under scrutiny – *i.e.*, to perform an imperfection-sensitivity study. In particular, it is essential to identify the most detrimental initial imperfection shape, in the sense that it leads to the lowest strengths. In this specific case, the aim is to find the initial imperfection shape, combining arbitrarily F_MT and F_m components, that leads to the lowest column F_MT strengths and failure loads. The elastic and elastic-plastic results presented were obtained by means of ANSYS non-linear shell finite element analyses SFEA (SAS 2009), using a model similar to that previously employed by Dinis *et al.* (2019, 2020a.b) – rounded corner and residual stress effects were disregarded, since they are known to practically cancel each other (*e.g.*, Ellobody & Young 2005).

4.1 Elastic Post-Buckling Strength – Most Detrimental Initial Geometrical Imperfections

Due to the presence of two competing buckling modes in columns affected by global-global interaction (critical F_MT and non-critical F_m modes), the commonly used approach of considering critical-mode initial imperfections ceases to be adequate. Indeed, in order to identify the most detrimental initial imperfection shape, it is necessary to determine and compare equilibrium paths of otherwise identical columns with initial geometrical imperfections that (i) span the whole critical-mode shape range and (ii) share a common amplitude. A systematic approach to identify the most detrimental initial geometrical imperfection shape was devised by Camotim & Dinis (2011) and accounts for the fact that the two competing buckling modes exhibit a single half-wave – it involves the performance of the following procedures:

(i) Determine "pure" critical buckling mode shapes, normalized to exhibit unit mid-span displacements: (i_1) a F_MT mode with a flange-lip corner downward vertical displacement equal to $v_{FT}=1$ mm and (i_2) two F_m modes with uniform horizontal displacements equal to $w_{Fm}=1$ mm (moving to the right) and $w_{Fm}=-1$ mm (moving to the left) – the need to consider the two F_m modes stems from the fact that they correspond to different post-buckling behaviors, as will be shown a bit ahead in the paper.

(ii) To scale the three "pure" modes, so that their amplitudes equal $L/1000$ (value commonly prescribed in cold-formed steel specifications).

(iii) A given initial geometrical imperfection shape is obtained by linearly combining the scaled buckling modes shapes, with coefficients $C_{FT.0}$ and $C_{Fm.0}$ satisfying the condition $(C_{FT.0})^2+(C_{Fm.0})^2=1$. A better visualization and "feel" of the initial imperfection shapes considered can be obtained by considering the unit radius half circle drawn on the $C_{FT.0}$-$C_{Fm.0}$ plane, as shown in Fig. 6(a)[4]. Each possible critical-mode imperfection shape corresponds to a point lying on this half circle, associated with an angle θ, measured from the horizontal ($C_{FT.0}$) axis and positive when counterclockwise – it defines a $C_{Fm.0}/C_{FT.0}$ ratio, where $C_{FT.0}=cos\theta$ and $D_{Fm.0}=sin\theta$. Fig. 6(b) shows the pure FT and F_m initial imperfection shapes ($\theta=0^o$; $\theta=90^o$; $\theta=-90^o$).

After having defined the full set of possible critical-mode initial geometrical imperfections shapes, it becomes possible to compare the elastic post-buckling behaviors of columns containing them, in order to (i) obtain numerical evidence of the occurrence of G-G interaction and (ii) identify the most detrimental

[4] Since the column F_MT post-buckling behavior is symmetric, it suffices to consider the half circle displayed in Fig. 6(a).

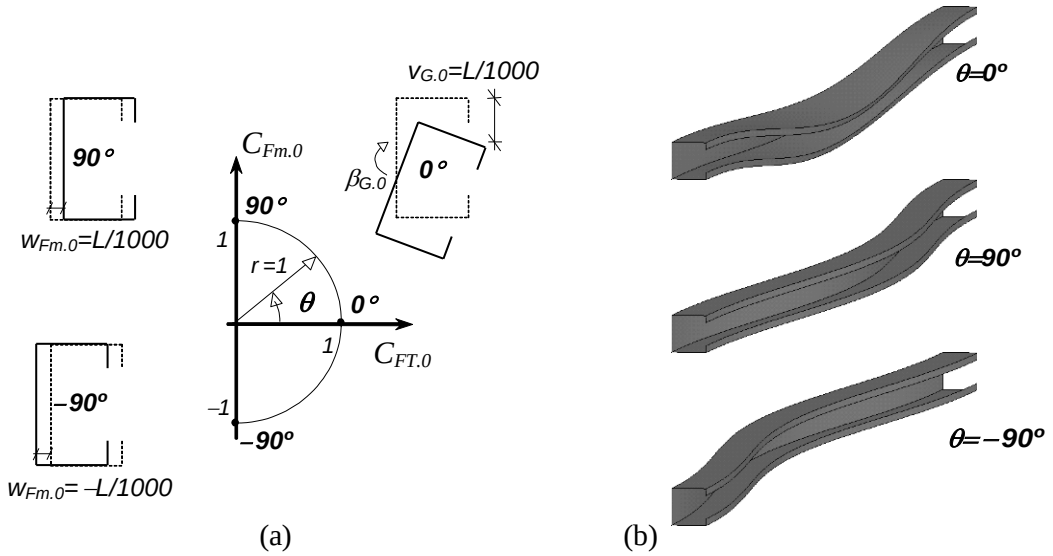

Figure 6. (a) Initial imperfection representation in the $C_{FT.0}$–$C_{Fm.0}$ plane and (b) initial imperfection shapes for θ=0º, ±90º

initial imperfection shape – this study considers initial imperfections corresponding to 15º intervals, *i.e.*, θ=0-±15-±30-±45-±60-±75-±90º.

The equilibrium paths P/P_{cr} vs. γ (γ is the mid-span torsional rotation) and P/P_{cr} vs. d_m/t (d_m is the mid-span translation due to minor-axis bending) displayed in Figs. 7(a_1)-(a_3) and 7(b_1)-(b_3), respectively, concern C_4 columns (β_{FT}=8.68) with lengths L_2, L_5 and L_6 (*i.e.*, experiencing three different levels of G-G interaction – R_G=1.50;1.14;1.01), and containing the 13 distinct initial geometrical imperfections dealt with in this work. As for Figs. 8(a)-(b), they show (i) four post-buckling equilibrium paths P/P_{cr} vs. γ and P/P_{cr} *vs.* d_m/t, already displayed in Fig. 7(a_1)-(b_1) and 7(a_3)-(b_3), concerning C_4 columns with lengths L_2 or L_7 and θ=45º initial geometrical imperfections, and also (ii) the evolution of the column mid-span cross-section deformed configuration as loading progresses. The close observation of these post-buckling results prompts the following remarks:

(i) The L_2 column equilibrium paths P/P_{cr} vs. γ corresponding to θ=0-±15-±30-±45-±60-±75º exhibit the expected stable behavior and merge into a common curve, associated with clockwise mid-span torsional rotations. Their post-critical strengths are ordered according to the amplitude of the F_m initial imperfection component, *i.e.*, the lowest and highest post-critical strengths correspond to the θ=0º and θ=±75º initial imperfections – naturally, the most detrimental initial imperfection shape is the "pure" F_MT one (θ=0º). Moreover, the equilibrium paths P/P_{cr} *vs.* d_m/t of the five columns with positive θ values exhibit a d_m reversal (from positive to negative) that occurs for P/P_{cr}≈0.85 – this does not happen for the five columns with negative θ values (d_m is always negative)[5]. As clearly shown by Dinis *et al.* (2020b), by means of Generalized Beam Theory (GBT) geometrically non-linear analyses, the difference between the columns having imperfections with positive and negative θ values stems from effective centroid shift effects due to the stress redistribution occurring in the (singly symmetric) lipped channel cross-section, mostly due to the warping stresses. The weakening of the flanges moves the effective centroid towards the web and the ensuing load eccentricity causes d_m translations to the left (negative) that either oppose (columns with θ>0 – d_m reversal) or reinforce (columns with θ<0 – no d_m reversal) those coming from the initial imperfections.

[5] Obviously, the θ=0º column also does not exhibit d_m reversal, since d_m≈0 prior to P/P_{cr}≈0.85.

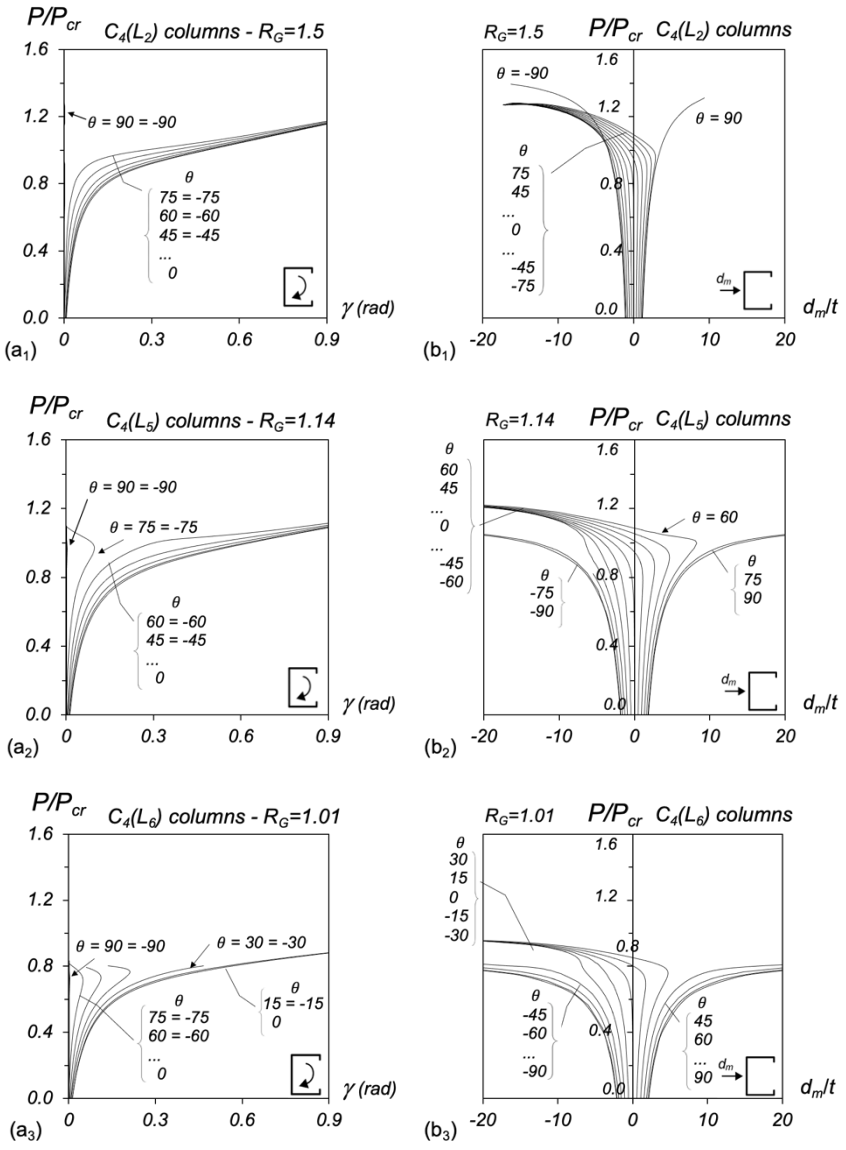

Figure 7: Elastic equilibrium paths (a) P/P_{cr} *vs.* γ and (b) P/P_{cr} *vs.* d_m/t of C_4 columns with lengths (1) L_2, (2) L_5 and (3) L_6

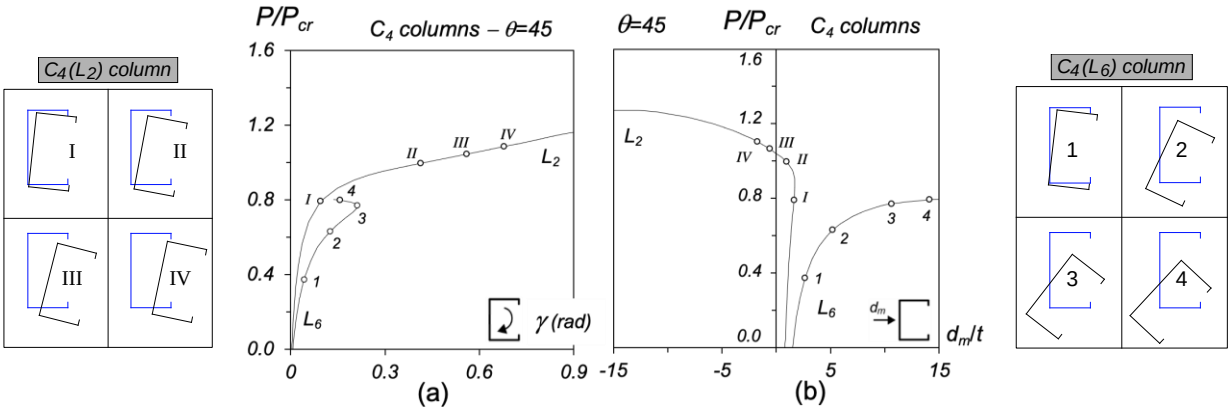

Figure 8: C_4 columns with lengths L_2 or L_6 and θ=45º initial imperfections: elastic equilibrium paths (a) P/P_{cr} *vs.* γ and (b) P/P_{cr} *vs.* d_m/t, and mid-span cross-section deformed configuration evolution along those equilibrium paths

(ii) The L_2 column P/P_{cr} vs. γ and P/P_{cr} *vs.* d_m/t equilibrium paths concerning θ=90º and θ=−90º ("pure" F_m initial geometrical imperfections) are identical and clearly different from the remaining ones – they correspond to a "singular" post-buckling behavior. Indeed, these columns exhibit virtually no F_MT deformations (only F_m ones) and their common post-critical strength is always the highest one – note that no effective centroid shift effects occur, due to the absence of F_MT deformations.

(iii) The post-buckling behaviors of the L_5 and L_6 columns are markedly different from their L_2 column counterpart, due to the fact that their R_G values are significantly lower (1.14 and 1.01 vs. 1.50). First of all, the post-critical strength is visibly smaller, which stems from the larger d_m values and reflects the presence of G-G (F_MT-F_m) interaction, naturally more relevant in the L_6 columns – this interaction amplifies the d_m values due to the initial geometrical imperfections and effective centroid shifts. As before, the P/P_{cr} vs. γ and P/P_{cr} *vs.* d_m/t equilibrium paths concerning θ=90º and θ=−90º are identical and clearly different from the remaining ones. However, reflecting the strength erosion caused by the G-G interaction, their common post-critical strength is no longer the highest one – in fact, it is the lowest one for the L_6 columns (even if this cannot be very clearly observed in Figs. 7(a_3) and 7(b_3)).

(iv) In the L_5 columns with θ=±75º and L_6 columns with θ=±30-±45-±60-±75º, the mid-span cross-section F_MT deformations cease to grow, rather abruptly, at a given applied load level, while the F_m deformations continue to grow – this means that this cross-section deformed configuration becomes progressively "more akin" to the F_m buckling mode shape. This feature is illustrated in Figs. 8(a)-(b), which compare the equilibrium paths and mid-span cross-section deformed configurations of the L_2 and L_6 columns with θ=45º. In the L_6 column, note the difference between the mid-span cross-section deformed configurations corresponding to the equilibrium states 3 and 4: while the F_MT deformations are practically the same, the F_m translations are quite different (the latter is much larger).

(v) It can be concluded that, depending on the column R_G value, the most detrimental initial geometrical imperfection shape may be either the "pure" F_MT buckling mode (θ=0º) or the "pure" F_m buckling mode (θ=90º or θ=−90º). Since it is often impossible to know, beforehand, which is the most detrimental initial imperfection shape, it was decided to consider both of them in the parametric study presented in Section 5, intended to gather failure load data of columns buckling in F_MT modes.

(vi) More in-depth knowledge on the mechanics of the coupling phenomenon under consideration in this work is currently being sought by the authors, through GBT geometrically non-linear analyses of columns with various cross-section dimensions and undergoing several levels of G-G interaction (R_G values) – the outcome of this search/investigation will be reported in the near future.

4.2 Elastic-Plastic Post-Buckling and Strength

As noted above, it was decided to determine failure loads concerning C columns containing both "pure" F_MT and "pure" F_m initial geometrical imperfections (amplitude L/1000) – recall that, depending on the particular column under scrutiny, either failure load can be the lowest one. In order to illustrate the type of results obtained, Figs. 9(a)-(b) show the elastic-plastic equilibrium paths P/P_{cr} *vs.* d_m/t of C_4 columns with (i) lengths L_4 or L_6, (ii) pure F_MT or F_m initial imperfections and (iii) 3 yield stresses ($f_y/f_{cr.FT}$≈1.1;2.2;3.3 – the elastic equilibrium paths correspond to $f_y/f_{cr.FT}=\infty$) – the failure loads obtained are identified by the white circles. Moreover, these figures also include the failure modes and plastic strains at collapse of the columns analyzed with $f_y/f_{cr.FT}$≈2.2 – the failure modes corresponding to F_MT and F_m initial imperfections are identified by letters "**A**" and "**B**", respectively, and have clearly visible different features: while the former failure mode exhibits plastic strains at top and bottom web-flange corner regions of the mid-span and end cross-sections, the latter one involves the full yielding of those cross-sections. The observation of these figures shows that:

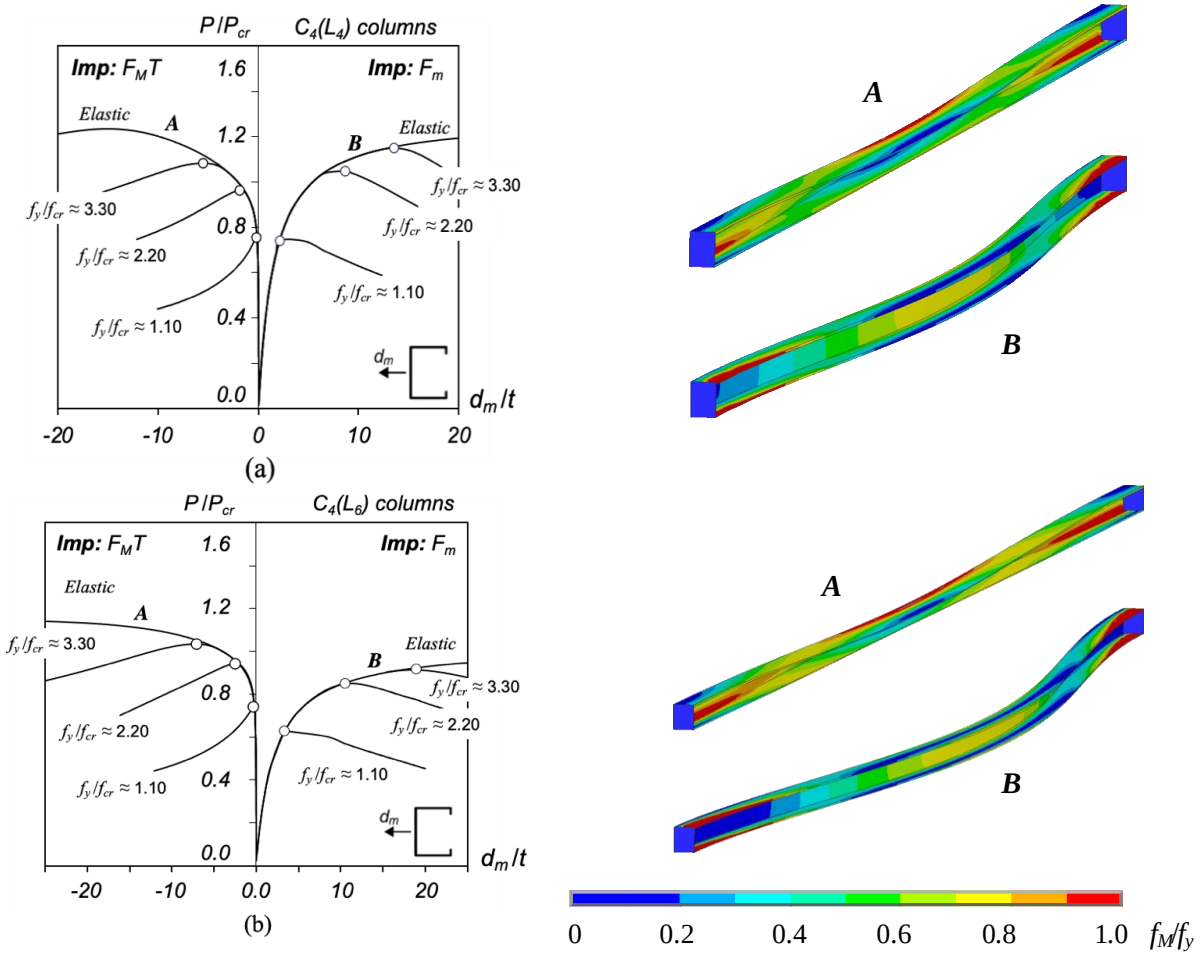

Figure 9: Elastic-plastic P/P_{cr} *vs.* d_m/t equilibrium paths and failure modes plus von Mises stresses f_M at collapse (for $f_y/f_{cr.FT}\approx 2.2$) of C_4 columns with F_MT or F_m initial imperfections, yield stresses such that $f_y/f_{cr.FT}\approx 1.1; 2.2; 3.3; \infty$) and lengths (a) L_4 or (b) L_6

(i) In the L_4 columns, the failure loads obtained for F_MT initial imperfections are either a bit smaller ($f_y/f_{cr.FT}\approx 2.2; 3.3$) or practically identical ($f_y/f_{cr.FT}\approx 1.1$) to those obtained for F_m initial imperfections.

(ii) In the L_6 columns, conversely, the failure loads obtained for F_m initial imperfections are always visibly smaller than those obtained for F_MT initial imperfections. Unlike in the L_4 columns, the difference is highest for $f_y/f_{cr.FT}\approx 1.1$ and then decreases as the yield stress grows.

5. Failure Load Data for Columns Undergoing Global-Global Interaction

In order to be able to address the DSM-based design of fixed-ended CFS C columns affected by different levels of G-G interaction, it is indispensable to begin by gathering a reasonably extensive failure load set concerning columns under these circumstances. The failure loads obtained in this work correspond to columns with the 48 geometries (combinations of b_w, b_f, b_l, t and L) given in Table 2, all associated with F_MT critical bucking, and five yield stresses (f_y=150; 300; 450; 600; 750 MPa), which enable covering a wide critical slenderness (λ_{FT}) range. Although this equals a total of 240 different columns, 480 failure loads are determined, as each column is analyzed with two initial geometrical imperfections: "pure" F_MT and F_m imperfections – naturally, only the lowest one is retained for design purposes. The full set of failure loads obtained is presented, in tabular form, in Annex A.

6. DSM Design

Fig. 10(a) plots, against λ_{FT}, the C column P_u/P_{nFT} values obtained in this work – they are also given in the table included in Annex A. As for Fig. 10(b), it plots, against the buckling load ratio R_G, the subset of P_u/P_{nFT} values concerning columns such that $\lambda_{FT}>1.5$ – the R_G values are also given in the table of Annex A. Both figures include the P_u/P_{nFT} statistical indicators (averages, standard deviations and maximum/minimum values). The observation of these two figures prompts the following remarks:

(i) As anticipated (see Fig. 3(b)), Eqs. (2)-(4) are unable to predict adequately the failure loads of the C columns affected by G-G mode interaction. Indeed, the P_u/P_{nFT} average (0.905), standard deviation (0.170) and minimum value (0.447) reflect a very poor prediction quality, combined a very large percentage of failure load overestimations (61.5%). This quality falls even lower if only columns with $\lambda_{FT}>1.5$ are considered: the above indicators become 0.848, 0.161, 0.477 and 78.2%, respectively. Moreover, it is also clear that the amount of failure load overestimation grows with λ_{FT}.

(ii) As also anticipated, Fig. 10(b) clearly shows that the amount of failure load overestimation is closely linked to the buckling load ratio R_G value – indeed, it is highest for $R_G\approx1.0$, remains meaningful up to $R_G\approx1.5$ and practically ceases to occur for $R_G>1.5$.

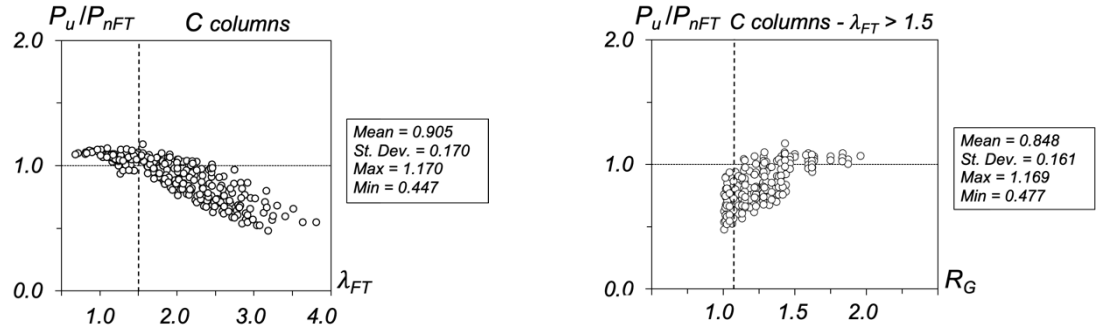

(a) (b)

Figure 10: Plots (a) P_u/P_{nFT} vs. λ_{FT}, for all the C columns analyzed, and (b) P_u/P_{nFT} vs. R_G, for the columns with $\lambda_{FT}>1.5$

Figs. 10(a)-(b) are qualitatively and quantitatively very similar to those reported by Dinis *et al.* (2020a), in the context of fixed-ended U columns undergoing F_MT-F_m interaction – in both cases, it is very clear (i) the very poor failure load prediction quality provided by P_{nFT} (see Eqs. (2)-(4)) and (ii) the decisive role played by G-G (F_MT-F_m) interaction in this poor performance. Therefore, it makes all the sense to begin by assessing whether the DSM-based design approach developed and proposed by these authors can be also used to predict efficiently the failure loads of C columns buckling in F_MT modes and failing in F_MT-F_m interactive modes – recall that an overview of this design approach, cast in the form expressed by Eqs. (5)-(8), was provided in Section 2.

In order to illustrate the failure load prediction quality achieved by Eqs. (5)-(8) when applied to the columns analyzed in this work (the majority of which are affected by G-G interaction), Figs. 11(a)-(f) (i) plot, against λ_{FT}, the P_u/P_y values (recall that P_u is the lowest of $P_{u.FT}$ and $P_{u.Fm}$) concerning the C_3 columns (β_{FT}=4.82) with lengths L_1-L_6 (R_G=1.87; 1. 62; 1. 41; 1. 23; 1. 16; 1.08), and (ii) compare those plots with the DSM-based strength curves defined by Eqs. (2)-(4) and (5)-(8) (P_{nFT} and $P_{nFT\text{-}G}$ – dashed and solid lines, respectively). It is clear that all P_u/P_y values are well predicted by the $P_{nFT\text{-}G}/P_y$ strength curves – indeed, they always provide rather accurate failure load underestimations, regardless of the R_G value (*i.e.*, the F_MT-F_m interaction level). On the other hand, those same P_u/P_y values are consistently and progressively overestimated by the P_{nFT}/P_y strength curves as R_G gradually drops below 1.5.

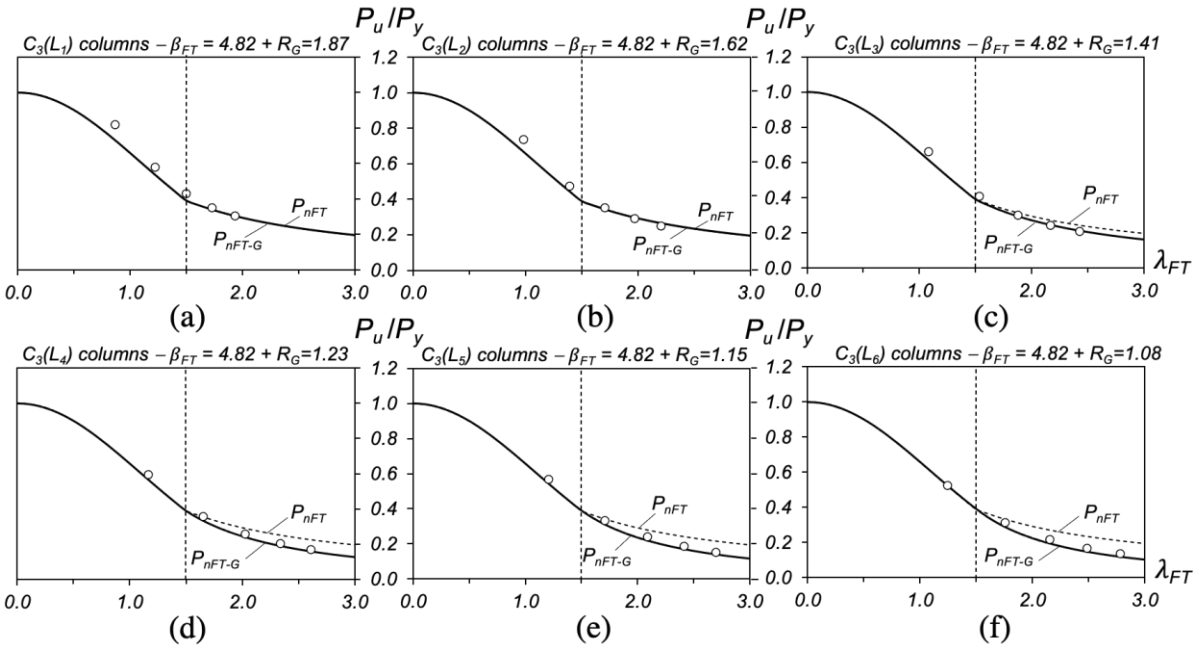

Figure 11: Comparison between the DSM strength curves P_{nFT}/P_y and P_{nFT-G}/P_y respectively proposed by Dinis *et al.* (2020b) and Dinis *et al.* (2020a), and the P_u/P_y values of C_3 columns with (a) L_1, (b) L_2, (c) L_3, (d) L_4, (e) L_5 and (f) L_6 lengths

Table A, included in Annex A, provides the whole set of numerical failure-to-predicted failure load ratios $P_{u.FT}/P_{nFT-G}$ and $P_{u.Fm}/P_{nFT-G}$ concerning the fixed-ended C columns analyzed in this work, as well as the values of the relevant quantities involved in their calculation, namely the column buckling load ratios R_G. In order to assess the overall performance and merits of Eqs. (5)-(8) in predicting the fixed-ended C column failure loads, Figs. 12(a)-(b) plot, against λ_{FT}, the P_u/P_{nFT-G} ratios concerning (i) the C columns analyzed in this work and (ii) those reported by Dinis *et al.* (2020b), all failing in "pure" F_MT modes (their R_G values are all above 1.5). Both figures include the associated P_u/P_{nFT-G} statistical indicators (averages, standard deviations and maximum/minimum values). The comparison between Figs. 12(a)-(b) and 4(a)-(b) unveils the remarkable similarity of the P_u/P_{nFT-G} "clouds" concerning the U and C columns, which is quantitatively confirmed by the closeness between the corresponding statistical indicator pairs.

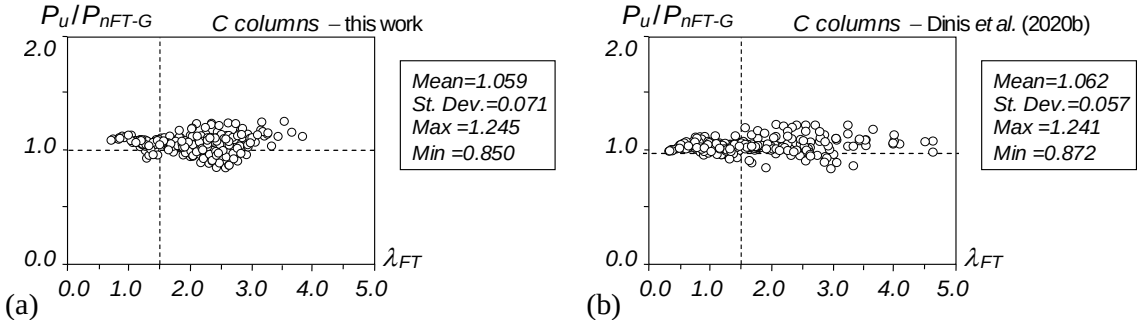

Figure 12: Plots P_u/P_{nFT-G} vs. λ_{FT} for the C columns (a) analyzed in this work and (b) reported by Dinis *et al.* (2020b)

In view of the content of the previous paragraph, it seems fair to conclude that the DSM-based design approach expressed by Eqs. (5)-(8), which was developed and proposed by Dinis *et al.* (2020a) on the sole basis of U column failure load data, also provides efficient failure load predictions for C columns buckling in F_MT modes and failing in either pure F_MT or F_MT-F_m interactive modes. In the next section, the

performance and merits of this DSM-based design approach will be assesses in the context of both U and C columns buckling in F_MT modes.

6.1 Merit and Reliability Assessment (for both U and C columns)

Table 3 provides, for all the fixed-ended U and C columns analyzed in this work and in previous studies (Dinis *et al.* 2020a,b), the failure load numbers (n) and $P_u/P_{nFT\text{-}G}$ statistical indicators, making a distinction between the columns such that $\lambda_{FT} \leq 1.5$ (those whose failure loads are estimated by the currently codified DSM global design curve) and such that $\lambda_{FT} > 1.5$ (those whose failure loads are predicted by the proposed DSM-based design approach – Eqs. (5)-(8)). These results prompt the following remarks:

(i) As mentioned earlier, the failure load prediction quality provided by the proposed DSM-based design approach is excellent. Indeed, the $P_u/P_{nFT\text{-}G}$ averages, standard deviations, maximum and minimum values read 1.057-0.078-1.245-0.850 for columns such that $\lambda_{FT} > 1.5$, which are very similar to those provided by the currently codified DSM global design curve for the columns with $\lambda_{FT} \leq 1.5$ (1.054-0.046-1.146-0.905) – this similarity holds for both the U (1.051-0.082-1.202-0.850 vs. 1.044-0.059-1.139-0.905) and C (1.062-0.076-1.245-0.850 vs. 1.057-0.039-1.146-0.933) columns.

(ii) Regardless of the β_{FT} and R_G value combination, the failure load prediction quality for the columns with $\lambda_{FT} > 1.5$ is always very high: the $P_u/P_{nFT\text{-}G}$ statistical indicators read 1.051-0.082-1.202-0.850 (U columns), 1.062-0.076-1.245-0.850 (C columns) and 1.057-0.078-1.245-0.850 (U and C columns).

(iii) In view of the content of the above two items, it can be rightfully stated that the DSM-based design approach expressed by Eqs. (5)-(8)) ensures a high prediction quality for the numerical failure loads of fixed-ended CFS U and C columns buckling in F_MT modes (those analyzed so far, either in this work or in previous studies by Dinis *et al.* (2020a,b)).

Table 3: Failure load numbers (n) and $P_u/P_{nFT\text{-}G}$ statistical indicators concerning the fixed-ended U and C columns analyzed in this work and in previous studies (Dinis *et al.* 2020a,b)

Parameter	U columns				C columns				All columns	
	Dinis *et al.* (2020b)		Dinis *et al.* (2020a)		Dinis *et al.* (2020b)		This Work			
λ_{FT}	≤ 1.5	> 1.5	≤ 1.5	> 1.5	≤ 1.5	> 1.5	≤ 1.5	> 1.5	≤ 1.5	> 1.5
n	29	61	51	184	128	142	64	176	272	563
Average	1.064	1.101	1.033	1.034	1.056	1.067	1.060	1.059	1.054	1.057
Sd. Dev.	0.029	0.071	0.069	0.078	0.037	0.071	0.043	0.079	0.046	0.078
Max	1.125	1.202	1.139	1.182	1.146	1.241	1.128	1.245	1.146	1.245
Min	1.017	0.850	0.905	0.854	0.952	0.872	0.933	0.850	0.905	0.850

Next, the reliability of the failure load predictions provided by the proposed DSM-based design approach is assessed in this section, through the determination of the LRFD (Load and Resistance Factor Design) resistance factors ϕ associated with the numerical failure loads obtained for the U and C columns analyzed in this work and in the previous studies reported by Dinis *et al.* (2020a,b). In particular, it is intended to check whether values equal or higher than ϕ_c=0.85 are achieved – this is the value recommended by the current North American Specification (AISI 2016) for compression members. According to this specification (Chapter K – Section K2.1.1), ϕ can be determined using the expression

$$\phi = C_\phi (M_m F_m P_m)\, e^{-\beta_0 \sqrt{V_M^2 + V_F^2 + C_P V_P^2 + V_Q^2}} \qquad \text{with} \qquad C_P = \left(1 + \frac{1}{n}\right)\frac{m}{m-2} \tag{9}$$

where (i) C_ϕ is a calibration coefficient (C_ϕ=1.52 for LRFD), (ii) M_m=1.10 and F_m=1.00 are the mean values of the material and fabrication factors, respectively, (iii) β_0 is the target reliability index (β_0=2.5 for structural members in LRFD), (iv) V_M=0.10, V_F=0.05 and V_Q=0.21 are the coefficients of variation of the material factor, fabrication factor and load effect, respectively, (v) C_P is a correction factor depending on the numbers of tests (n) and degrees of freedom (m=n–1), and (vi) P_m and V_P are the mean and coefficient of variation of the "exact"-to-predicted failure load ratios $P_u/P_{nFT\text{-}G}$.

Table 4 shows the n, C_P, P_m, V_P and ϕ values obtained from the $P_u/P_{nFT\text{-}G}$ values concerning the various sets of column numerical failure loads considered in his work. It can be observed that:

(i) The ϕ values obtained from the $P_{nFT\text{-}G}$ failure load estimates concerning the individual sets of U and C column are very similar (0.941 vs. 0.960) and well above the value prescribed by AISI (2016) for compression members (ϕ_c=0.85).

(ii) Naturally, $P_{nFT\text{-}G}$ estimates of all the available U and C column failure loads, jointly considered, lead to a ϕ value in between the previous two (ϕ=0.953).

(iii) In view of the content of the above two items, it can be concluded that the proposed DSM-based design approach provides very reliable failure load predictions for fixed-ended CFS U and C columns buckling in F_MT modes.

Table 4: LRFD ϕ values associated with the $P_{nFT\text{-}G}$ predictions of all the available column failure loads: (i) U columns reported by Dinis *et al.* (2020a,b), (ii) C columns analyzed in this work and reported by Dinis *et al.* (2020b), and (iii) all columns

Parameter	U columns			C columns			All columns
	Dinis *et al.* (2020b)	Dinis *et al.* (2020a)	Both	Dinis *et al.* (2020b)	This Work	Both	
n	90	235	325	270	240	510	835
m	89	234	324	269	239	509	834
C_P	1.034	1.013	1.009	1.011	1.013	1.006	1.004
P_m	1.089	1.034	1.049	1.062	1.059	1.061	1.056
V_P	0.057	0.074	0.073	0.054	0.067	0.061	0.066
ϕ	0.987	0.927	0.941	0.965	0.954	0.960	0.953

7. Concluding Remarks

This paper reported the most recent results of an ongoing numerical investigation on the post-buckling behavior, ultimate strength and DSM design of cold-formed steel moderately long columns experiencing interaction between major-axis flexural-torsional (critical) and minor-axis flexural buckling – this research effort was recently initiated by Dinis *et al.* (2020a), who unveiled and studied this coupling phenomenon in the context of fixed-ended plain channel (U) columns. In this work, the above pioneer study has been extended to cover also fixed-ended lipped channel (C) columns affected by different levels of the novel global-global (G-G) interaction or, to be more precise, flexural/torsional-flexural (F_MT-F_m) interaction. After providing an overview of the DSM-based design approach developed by Dinis *et al.* (2020a), in the sole context of fixed-ended U columns undergoing F_MT-F_m interaction, the paper addressed the selection of the C column geometries ensuring critical buckling in F_MT modes and a variable closeness of the F_MT and F_m buckling loads, as well as the identification of the most detrimental initial geometrical imperfection shape, *i.e.*, that leading to the lowest failure load. Then, ANSYS shell finite element models were employed to obtain the failure loads of the selected 240 C columns, which exhibit various cross-section dimensions, lengths and yield stresses, chosen to enable covering wide buckling load ratio (R_G) and F_MT flexural-torsional slenderness ranges (λ_{FT}). On the basis of these failure load data, together with the 270 fixed-

ended C column failure loads reported by Dinis *et al.* (2020b), it was possible to show that the DSM-based design approach developed and proposed by Dinis *et al.* (2020a), in the sole context of U columns, also provides efficient (safe, accurate and reliable) predictions of the failure loads of C columns failing in F_MT (pure) or F_MT-F_m (interactive) modes. In other words, it was shown that the above DSM-based design approach can handle adequately both U and C fixed-ended columns. Indeed, the $P_u/P_{nFT\text{-}G}$ values concerning all the U and C columns analyzed by Dinis *et al.* (2020a,b) and in this work lead to LRFD resistance factors higher than 0.94 (ϕ=0.94,0,96,0.95, respectively for the U, C and U+C columns), *i.e.*, well above the value recommended in AISI (2016) for compression members – ϕ_c=0.85.

The findings reported by Dinis *et al.* (2020a) and in this paper provide encouragement to extend the adopted methodology to columns with other cross-section shapes and/or end support conditions, thus paving the way for the development of a general and unified DSM-based approach for the design of CFS columns failing in F_MT (pure) or F_MT-F_m (interactive) modes.

References

AISC (American Institute of Steel Construction) (1986). *Load and Resistance Factor Design Specification for Structural Steel Buildings* (AISC 328:1986), Chicago IL.

AISI (American Iron and Steel Institute) (1986). *Cold-Formed Steel Design Manual*, Washington DC.

AISI (American Iron and Steel Institute) (1996). *Cold-Formed Steel Design Manual*, Washington DC.

AISI (American Iron and Steel Institute) (2016). *North American Specification (NAS) for the Design of Cold-Formed Steel Structural Members*, AISI-S100-16, Washington DC.

Bebiano R, Camotim D, Gonçalves R (2018). GBTUL 2.0 – a second-generation code for the GBT-based buckling and vibration analysis of thin-walled members, *Thin-Walled Structures*, **124**(March), 235-257.

Camotim D, Dinis PB (2011). Coupled instabilities with distortional buckling in cold-formed steel lipped channel columns, *Thin-Walled Structures*, **49**(5), 562-575.

Camotim D, Dinis PB, Landesmann A (2020). Behavior, failure and Direct Strength Method design of steel angle columns: geometrical simplicity vs. structural complexity, *Journal of Structural Engineering*, **146**(11), paper 04020226 (25 pages).

Camotim D, Dinis PB, Martins AD (2016). Direct Strength Method (DSM) − a general approach for the design of cold-formed steel structures, *Recent Trends in Cold-Formed Steel Construction*, C. Yu (ed.), Woodhead Publishing (Amsterdam − Series in Civil and Structural Engineering), 69-105.

Dinis PB, Camotim D, Landesmann A, Martins AD (2019). On the Direct Strength Method design of columns against global failure, *Thin-Walled Structures*, **139**(June), 242-270.

Dinis PB, Camotim D, Martins AD, Landesmann A (2020a). Global-global interaction in cold-formed steel channel columns: relevance, post-buckling behavior, strength and DSM design, *Website Proceedings of Structural Stability Research Council (SSRC) Annual Stability Conference* (Georgia, 21-24/4).

Dinis PB, Camotim D, Landesmann A, Martins AD (2020b). Improving the Direct Strength Method prediction of column flexural-torsional failure loads, *Thin-Walled Structures*, **148**(March), paper 106461 (18 pages).

Ellobody E, Young B (2005). Behavior of cold-formed steel plain angle columns, *Journal of Structural Engineering* (ASCE), **131**(3), 469-478.

Hancock GJ, Kwon YB, Bernard ES (1994). Strength design curves for thin-walled sections undergoing distortional buckling, *Journal of Construction Steel Research*, **31**(2-3), 169-186.

Swanson Analysis Systems Inc. (SAS) (2009). *Ansys Reference Manual* (vrs. 12).

Schafer BW (2008). Review: the direct strength method of cold-formed steel member design, *Journal of Constructional Steel Research*, **64**(7-8), 766-778.

Schafer BW (2019). Advances in the Direct Strength Method of cold-formed steel design, *Thin-Walled Structures*, **140**(July), 533-541.

Schafer BW, Peköz T (1998). Direct strength prediction of cold-formed steel members using numerical elastic buckling solutions, *Proceedings of 14th International Specialty Conference on Cold-Formed Steel Structures* (St. Louis, 15-16/10), W.W. Yu, R. LaBoube (eds.), 69-76.

Peköz T, Sümer O (1992). *Design Provisions for Cold-Formed Steel Columns and Beam-Column*, Research Report RP92-1, American Iron and Steel Institute, Washington DC.

Torabian S, Schafer BW (2018). Development and experimental validation of the Direct Strength Method for cold-formed steel beam-columns, *Journal of Structural Engineering* (ASCE), **144**(10), paper 04018175 (21 pages).

Ziemian R (editor) (2010). *Guide to Stability Design Criteria for Metal Structures* (6th edition), John Wiley & Sons, Hoboken.

ANNEX A

Table A: C columns buckling and failing in F_MT modes: (i) geometries, (ii) buckling stresses, (iii) failure loads, (iv) failure load predictions P_{nFT} and $P_{nFT\text{-}G}$, and (v) corresponding numerical-to-predicted failure loads ratios (mm, MPa, kN)

Column	Geometry			SFEA				DMS Design												
	$b_w \times b_f \times b_l \times t$	β_{FT}	L	f_y	$P_{u.FT}$	$P_{u.Fm}$	P_u	$f_{cr.FT}$	λ_{FT}	b	a	P_{nFT}	$\frac{P_u}{P_{nFT}}$	$f_{b.Fm}$	R_G	c	b	a	$P_{nFT\text{-}G}$	$\frac{P_u}{P_{nFT-G}}$
C1_L1	60×55×11×4	2.60	4800	150	80.0	89.0	80.0	115.0	1.14	0.87	0.55	75.08	1.07	157.8	1.37	1.077	1.23	0.64	75.08	1.07
		2.60	4800	300	94.2	117.5	94.2	115.0	1.62	0.87	0.55	94.82	0.99	157.8	1.37	1.077	1.23	0.64	92.28	1.02
		2.60	4800	450	102.0	125.3	102.0	115.0	1.98	0.87	0.55	119.32	0.85	157.8	1.37	1.077	1.23	0.64	107.81	0.95
		2.60	4800	600	107.1	128.7	107.1	115.0	2.28	0.87	0.55	140.45	0.76	157.8	1.37	1.077	1.23	0.64	120.39	0.89
		2.60	4800	750	111.5	130.5	111.5	115.0	2.55	0.87	0.55	159.39	0.70	157.8	1.37	1.077	1.23	0.64	131.15	0.85
C1_L2	60x×55×11×4	2.60	5000	150	77.8	85.5	77.8	110.0	1.17	0.87	0.55	73.24	1.06	145.5	1.32	1.175	1.33	0.67	73.24	1.06
		2.60	5000	300	90.7	109.7	90.7	110.0	1.65	0.87	0.55	93.01	0.98	145.5	1.32	1.175	1.33	0.67	88.94	1.02
		2.60	5000	450	96.8	116.6	96.8	110.0	2.02	0.87	0.55	117.04	0.83	145.5	1.32	1.175	1.33	0.67	101.87	0.95
		2.60	5000	600	102.0	119.2	102.0	110.0	2.34	0.87	0.55	137.78	0.74	145.5	1.32	1.175	1.33	0.67	112.16	0.91
		2.60	5000	750	105.4	121.0	105.4	110.0	2.61	0.87	0.55	156.35	0.67	145.5	1.32	1.175	1.33	0.67	120.86	0.87
C1_L3	60×55×11×4	2.60	5500	150	71.5	76.4	71.5	98.9	1.23	0.87	0.55	68.69	1.04	120.2	1.22	1.343	1.50	0.72	68.69	1.04
		2.60	5500	300	81.8	92.4	81.8	98.9	1.74	0.87	0.55	88.82	0.92	120.2	1.22	1.343	1.50	0.72	80.81	1.01
		2.60	5500	450	86.4	97.6	86.4	98.9	2.13	0.87	0.55	111.77	0.77	120.2	1.22	1.343	1.50	0.72	89.45	0.97
		2.60	5500	600	89.9	99.4	89.9	98.9	2.46	0.87	0.55	131.57	0.68	120.2	1.22	1.343	1.50	0.72	96.14	0.93
		2.60	5500	750	92.4	100.2	92.4	98.9	2.75	0.87	0.55	149.32	0.62	120.2	1.22	1.343	1.50	0.72	101.67	0.91
C1_L4	60×55×11×4	2.60	6000	150	65.9	67.7	65.9	89.4	1.30	0.87	0.55	64.21	1.03	101.0	1.13	1.511	1.67	0.77	64.21	1.03
		2.60	6000	300	74.0	79.2	74.0	89.4	1.83	0.87	0.55	85.02	0.87	101.0	1.13	1.511	1.67	0.77	72.44	1.02
		2.60	6000	450	77.4	82.5	77.4	89.4	2.24	0.87	0.55	106.99	0.72	101.0	1.13	1.511	1.67	0.77	77.50	1.00
		2.60	6000	600	79.7	84.0	79.7	89.4	2.59	0.87	0.55	125.94	0.63	101.0	1.13	1.511	1.67	0.77	81.30	0.98
		2.60	6000	750	81.2	84.8	81.2	89.4	2.90	0.87	0.55	142.93	0.57	101.0	1.13	1.511	1.67	0.77	84.38	0.96
C1_L5	60×55×11×4	2.60	6500	150	60.7	60.0	60.0	81.1	1.36	0.87	0.55	59.76	1.00	86.1	1.06	1.72	1.88	0.83	59.76	1.00
		2.60	6500	300	67.0	68.4	67.0	81.1	1.92	0.87	0.55	81.51	0.82	86.1	1.06	1.72	1.88	0.83	63.41	1.06
		2.60	6500	450	69.4	70.8	69.4	81.1	2.36	0.87	0.55	102.57	0.68	86.1	1.06	1.72	1.88	0.83	65.02	1.07
		2.60	6500	600	70.8	71.9	70.8	81.1	2.72	0.87	0.55	120.74	0.59	86.1	1.06	1.72	1.88	0.83	66.19	1.07
		2.60	6500	750	71.6	72.6	71.6	81.1	3.04	0.87	0.55	137.02	0.52	86.1	1.06	1.72	1.88	0.83	67.11	1.07
C1_L6	60×55×11×4	2.60	7000	150	55.8	53.2	53.2	73.8	1.43	0.87	0.55	55.35	0.96	74.2	1.01	1.971	2.00	0.88	55.35	0.96
		2.60	7000	300	60.7	59.5	59.5	73.8	2.02	0.87	0.55	78.24	0.76	74.2	1.01	1.971	2.00	0.88	55.95	1.06
		2.60	7000	450	62.3	61.4	61.4	73.8	2.47	0.87	0.55	98.46	0.62	74.2	1.01	1.971	2.00	0.88	55.95	1.10
		2.60	7000	600	63.1	62.3	62.3	73.8	2.85	0.87	0.55	115.90	0.54	74.2	1.01	1.971	2.00	0.88	55.95	1.11
		2.60	7000	750	63.4	62.7	62.7	73.8	3.19	0.87	0.55	131.53	0.48	74.2	1.01	1.971	2.00	0.88	55.95	1.12
C2_L1	100×60×10×3	6.32	3500	150	85.3	91.9	85.3	184.1	0.90	1.09	0.61	76.79	1.11	337.9	1.84	0.71	1.09	0.61	76.79	1.11
		6.32	3500	300	117.7	155.1	117.7	184.1	1.28	1.09	0.61	109.21	1.08	337.9	1.84	0.71	1.09	0.61	109.21	1.08
		6.32	3500	450	131.8	193.4	131.8	184.1	1.56	1.09	0.61	120.78	1.09	337.9	1.84	0.71	1.09	0.61	120.78	1.09
		6.32	3500	600	144.4	210.0	144.4	184.1	1.81	1.09	0.61	137.69	1.05	337.9	1.84	0.71	1.09	0.61	137.69	1.05
		6.32	3500	750	156.6	218.0	156.6	184.1	2.02	1.09	0.61	152.41	1.03	337.9	1.84	0.71	1.09	0.61	152.41	1.03
C2_L2	100×60×10×3	6.32	4500	150	71.6	79.4	71.6	128.5	1.08	1.09	0.61	66.26	1.08	204.8	1.59	0.71	1.09	0.61	66.26	1.08
		6.32	4500	300	90.0	117.4	90.0	128.5	1.53	1.09	0.61	82.56	1.09	204.8	1.59	0.71	1.09	0.61	82.56	1.09
		6.32	4500	450	102.2	129.7	102.2	128.5	1.87	1.09	0.61	99.30	1.03	204.8	1.59	0.71	1.09	0.61	99.30	1.03
		6.32	4500	600	112.9	135.0	112.9	128.5	2.16	1.09	0.61	113.20	1.00	204.8	1.59	0.71	1.09	0.61	113.20	1.00
		6.32	4500	750	121.2	137.7	121.2	128.5	2.42	1.09	0.61	125.30	0.97	204.8	1.59	0.71	1.09	0.61	125.30	0.97
C2_L3	100×60×10×3	6.32	5500	150	60.6	65.5	60.6	99.8	1.23	1.09	0.61	57.57	1.05	137.1	1.37	1.073	1.45	0.70	57.57	1.05
		6.32	5500	300	74.0	84.9	74.0	99.8	1.73	1.09	0.61	71.94	1.03	137.1	1.37	1.073	1.45	0.70	68.26	1.08
		6.32	5500	450	83.3	90.3	83.3	99.8	2.12	1.09	0.61	86.53	0.96	137.1	1.37	1.073	1.45	0.70	76.27	1.09
		6.32	5500	600	89.7	92.6	89.7	99.8	2.45	1.09	0.61	98.64	0.91	137.1	1.37	1.073	1.45	0.70	82.52	1.09
		6.32	5500	750	93.5	93.8	93.5	99.8	2.74	1.09	0.61	109.18	0.86	137.1	1.37	1.073	1.45	0.70	87.72	1.07
C2_L4	100×60×10×3	6.32	6000	150	56.2	59.6	56.2	90.3	1.29	1.09	0.61	53.89	1.04	115.2	1.28	1.25	1.63	0.76	53.89	1.04
		6.32	6000	300	67.9	73.0	67.9	90.3	1.82	1.09	0.61	68.13	1.00	115.2	1.28	1.25	1.63	0.76	61.32	1.11
		6.32	6000	450	75.3	76.7	75.3	90.3	2.23	1.09	0.61	81.94	0.92	115.2	1.28	1.25	1.63	0.76	66.10	1.14
		6.32	6000	600	79.7	78.4	78.4	90.3	2.58	1.09	0.61	93.41	0.84	115.2	1.28	1.25	1.63	0.76	69.72	1.12
		6.32	6000	750	81.8	79.3	79.3	90.3	2.88	1.09	0.61	103.39	0.77	115.2	1.28	1.25	1.63	0.76	72.66	1.09
C2_L5	100×60×10×3	6.32	7000	150	49.3	47.8	47.8	76.6	1.40	1.09	0.61	47.58	1.01	84.7	1.11	1.575	1.95	0.86	47.58	1.01
		6.32	7000	300	57.5	55.1	55.1	76.6	1.98	1.09	0.61	62.29	0.88	84.7	1.11	1.575	1.95	0.86	49.01	1.12
		6.32	7000	450	61.3	57.2	57.2	76.6	2.42	1.09	0.61	74.92	0.76	84.7	1.11	1.575	1.95	0.86	49.47	1.16
		6.32	7000	600	62.7	58.2	58.2	76.6	2.80	1.09	0.61	85.40	0.68	84.7	1.11	1.575	1.95	0.86	49.80	1.17
		6.32	7000	750	63.0	58.7	58.7	76.6	3.13	1.09	0.61	94.53	0.62	84.7	1.11	1.575	1.95	0.86	50.05	1.17
C2_L6	100×60×10×3	6.32	7500	150	46.4	43.1	43.1	71.5	1.45	1.09	0.61	44.88	0.96	73.8	1.03	1.841	2.00	0.88	44.88	0.96
		6.32	7500	300	52.9	48.5	48.5	71.5	2.05	1.09	0.61	59.99	0.81	73.8	1.03	1.841	2.00	0.88	45.17	1.07
		6.32	7500	450	55.2	50.1	50.1	71.5	2.51	1.09	0.61	72.16	0.69	73.8	1.03	1.841	2.00	0.88	45.17	1.11
		6.32	7500	600	55.7	50.9	50.9	71.5	2.90	1.09	0.61	82.25	0.62	73.8	1.03	1.841	2.00	0.88	45.17	1.13
		6.32	7500	750	55.7	51.3	51.3	71.5	3.24	1.09	0.61	91.05	0.56	73.8	1.03	1.841	2.00	0.88	45.17	1.14

Column	Geometry			SFEA				DMS Design												
	$b_w \times b_f \times b_l \times t$	β_{FT}	L	f_y	$P_{u.FT}$	$P_{u.Fm}$	P_u	$f_{cr.FT}$	λ_{FT}	b	a	P_{nFT}	$\frac{P_u}{P_{nFT}}$	$f_{b.Fm}$	R_G	c	b	a	$P_{nFT\text{-}G}$	$\frac{P_u}{P_{nFT-G}}$
C3_L1	120×80×15×5	4.82	4500	150	190.4	199.9	190.4	200.2	0.87	1.00	0.58	169.91	1.12	374.5	1.87	0.71	1.00	0.58	169.91	1.12
		4.82	4500	300	269.3	357.8	269.3	200.2	1.22	1.00	0.58	248.35	1.08	374.5	1.87	0.71	1.00	0.58	248.35	1.08
		4.82	4500	450	300.6	450.2	300.6	200.2	1.50	1.00	0.58	272.25	1.10	374.5	1.87	0.71	1.00	0.58	272.25	1.10
		4.82	4500	600	326.6	494.4	326.6	200.2	1.73	1.00	0.58	314.30	1.04	374.5	1.87	0.71	1.00	0.58	314.30	1.04
		4.82	4500	750	352.7	518.9	352.7	200.2	1.94	1.00	0.58	351.43	1.00	374.5	1.87	0.71	1.00	0.58	351.43	1.00
C3_L2	120×80×15×5	4.82	5500	150	171.7	185.6	171.7	154.8	0.98	1.00	0.58	154.98	1.11	250.9	1.62	0.71	1.00	0.58	154.98	1.11
		4.82	5500	300	221.2	292.6	221.2	154.8	1.39	1.00	0.58	206.62	1.07	250.9	1.62	0.71	1.00	0.58	206.62	1.07
		4.82	5500	450	246.6	332.3	246.6	154.8	1.70	1.00	0.58	239.35	1.03	250.9	1.62	0.71	1.00	0.58	239.35	1.03
		4.82	5500	600	269.8	351.0	269.8	154.8	1.97	1.00	0.58	276.41	0.98	250.9	1.62	0.71	1.00	0.58	276.41	0.98
		4.82	5500	750	290.5	360.5	290.5	154.8	2.20	1.00	0.58	309.06	0.94	250.9	1.62	0.71	1.00	0.58	309.06	0.94
C3_L3	120×80×15×5	4.82	6500	150	153.5	167.2	153.5	127.8	1.08	1.00	0.58	142.26	1.08	179.7	1.41	0.991	1.28	0.66	142.26	1.08
		4.82	6500	300	189.2	228.7	189.2	127.8	1.53	1.00	0.58	177.55	1.07	179.7	1.41	0.991	1.28	0.66	176.49	1.07
		4.82	6500	450	210.0	249.5	210.0	127.8	1.88	1.00	0.58	217.49	0.97	179.7	1.41	0.991	1.28	0.66	204.21	1.03
		4.82	6500	600	227.2	258.3	227.2	127.8	2.17	1.00	0.58	251.17	0.90	179.7	1.41	0.991	1.28	0.66	226.48	1.00
		4.82	6500	750	240.3	262.9	240.3	127.8	2.42	1.00	0.58	280.84	0.86	179.7	1.41	0.991	1.28	0.66	245.41	0.98
C3_L4	120×80×15×5	4.82	7500	150	138.7	141.5	138.7	109.9	1.17	1.00	0.58	131.32	1.06	135.0	1.23	1.322	1.61	0.75	131.32	1.06
		4.82	7500	300	165.4	180.9	165.4	109.9	1.65	1.00	0.58	164.66	1.00	135.0	1.23	1.322	1.61	0.75	155.20	1.07
		4.82	7500	450	180.6	192.2	180.6	109.9	2.02	1.00	0.58	201.70	0.90	135.0	1.23	1.322	1.61	0.75	167.93	1.08
		4.82	7500	600	191.3	197.0	191.3	109.9	2.34	1.00	0.58	232.93	0.82	135.0	1.23	1.322	1.61	0.75	177.59	1.08
		4.82	7500	750	198.1	199.7	198.1	109.9	2.61	1.00	0.58	260.45	0.76	135.0	1.23	1.322	1.61	0.75	185.46	1.07
C3_L5	120×80×15×5	4.82	8000	150	132.2	133.2	132.2	103.0	1.21	1.00	0.58	126.39	1.05	118.3	1.15	1.467	1.76	0.79	126.39	1.05
		4.82	8000	300	155.2	162.0	155.2	103.0	1.71	1.00	0.58	159.41	0.97	118.3	1.15	1.467	1.76	0.79	144.57	1.07
		4.82	8000	450	167.6	170.2	167.6	103.0	2.09	1.00	0.58	195.27	0.86	118.3	1.15	1.467	1.76	0.79	151.89	1.10
		4.82	8000	600	175.3	174.1	174.1	103.0	2.41	1.00	0.58	225.51	0.77	118.3	1.15	1.467	1.76	0.79	157.31	1.11
		4.82	8000	750	179.7	176.2	176.2	103.0	2.70	1.00	0.58	252.15	0.70	118.3	1.15	1.467	1.76	0.79	161.65	1.09
C3_L6	120×80×15×5	4.82	8500	150	126.1	121.5	121.5	97.0	1.24	1.00	0.58	121.71	1.00	105.1	1.08	1.643	1.93	0.85	121.71	1.00
		4.82	8500	300	145.9	145.2	145.2	97.0	1.76	1.00	0.58	154.70	0.94	105.1	1.08	1.643	1.93	0.85	133.36	1.09
		4.82	8500	450	155.4	151.9	151.9	97.0	2.15	1.00	0.58	189.50	0.80	105.1	1.08	1.643	1.93	0.85	135.21	1.12
		4.82	8500	600	160.7	154.9	154.9	97.0	2.49	1.00	0.58	218.84	0.71	105.1	1.08	1.643	1.93	0.85	136.54	1.13
		4.82	8500	750	163.2	156.6	156.6	97.0	2.78	1.00	0.58	244.70	0.64	105.1	1.08	1.643	1.93	0.85	137.57	1.14
C4_L1	140×70×10×3.5	8.68	3400	150	139.3	140.3	139.3	291.4	0.72	1.23	0.64	126.97	1.10	459.5	1.58	0.71	1.23	0.64	126.97	1.10
		8.68	3400	300	231.0	255.8	231.0	291.4	1.01	1.23	0.64	204.73	1.13	459.5	1.58	0.71	1.23	0.64	204.73	1.13
		8.68	3400	450	269.5	331.8	269.5	291.4	1.24	1.23	0.64	247.57	1.09	459.5	1.58	0.71	1.23	0.64	247.57	1.09
		8.68	3400	600	289.5	367.0	289.5	291.4	1.43	1.23	0.64	266.11	1.09	459.5	1.58	0.71	1.23	0.64	266.11	1.09
		8.68	3400	750	304.4	381.3	304.4	291.4	1.60	1.23	0.64	282.74	1.08	459.5	1.58	0.71	1.23	0.64	282.74	1.08
C4_L2	140×70×10×3.5	8.68	4000	150	131.5	133.9	131.5	223.1	0.82	1.23	0.64	118.87	1.11	334.3	1.50	0.71	1.23	0.64	118.87	1.11
		8.68	4000	300	195.9	228.1	195.9	223.1	1.16	1.23	0.64	179.42	1.09	334.3	1.50	0.71	1.23	0.64	179.42	1.09
		8.68	4000	450	221.4	277.3	221.4	223.1	1.42	1.23	0.64	203.12	1.09	334.3	1.50	0.71	1.23	0.64	203.12	1.09
		8.68	4000	600	238.7	315.9	238.7	223.1	1.64	1.23	0.64	220.16	1.08	334.3	1.50	0.71	1.23	0.64	220.16	1.08
		8.68	4000	750	254.3	309.3	254.3	223.1	1.83	1.23	0.64	239.89	1.06	334.3	1.50	0.71	1.23	0.64	239.89	1.06
C4_L3	140×70×10×3.5	8.68	4500	150	124.2	126.4	124.2	185.6	0.90	1.23	0.64	112.30	1.11	264.8	1.43	0.93	1.45	0.70	112.30	1.11
		8.68	4500	300	172.7	200.4	172.7	185.6	1.27	1.23	0.64	160.14	1.08	264.8	1.43	0.93	1.45	0.70	160.14	1.08
		8.68	4500	450	193.2	232.6	193.2	185.6	1.56	1.23	0.64	175.99	1.10	264.8	1.43	0.93	1.45	0.70	174.55	1.11
		8.68	4500	600	210.1	246.1	210.1	185.6	1.80	1.23	0.64	196.59	1.07	264.8	1.43	0.93	1.45	0.70	188.90	1.11
		8.68	4500	750	224.5	252.2	224.5	185.6	2.01	1.23	0.64	214.21	1.05	264.8	1.43	0.93	1.45	0.70	200.84	1.12
C4_L4	140×70×10×3.5	8.68	5500	150	109.0	106.6	106.6	138.6	1.04	1.23	0.64	100.13	1.06	177.6	1.28	1.242	1.76	0.80	100.13	1.06
		8.68	5500	300	138.9	151.1	138.9	138.6	1.47	1.23	0.64	127.31	1.09	177.6	1.28	1.242	1.76	0.80	127.31	1.09
		8.68	5500	450	156.0	165.4	156.0	138.6	1.80	1.23	0.64	147.05	1.06	177.6	1.28	1.242	1.76	0.80	133.39	1.17
		8.68	5500	600	169.2	171.2	169.2	138.6	2.08	1.23	0.64	164.26	1.03	177.6	1.28	1.242	1.76	0.80	138.03	1.23
		8.68	5500	750	177.9	174.2	174.2	138.6	2.33	1.23	0.64	178.98	0.97	177.6	1.28	1.242	1.76	0.80	141.74	1.23
C4_L5	140×70×10×3.5	8.68	6500	150	95.3	92.3	92.3	111.2	1.16	1.23	0.64	89.55	1.03	127.2	1.14	1.478	2.00	0.88	89.55	1.03
		8.68	6500	300	117.0	114.8	114.8	111.2	1.64	1.23	0.64	109.87	1.04	127.2	1.14	1.478	2.00	0.88	102.47	1.12
		8.68	6500	450	129.8	121.9	121.9	111.2	2.01	1.23	0.64	128.41	0.95	127.2	1.14	1.478	2.00	0.88	102.51	1.19
		8.68	6500	600	137.2	124.9	124.9	111.2	2.32	1.23	0.64	143.44	0.87	127.2	1.14	1.478	2.00	0.88	102.54	1.22
		8.68	6500	750	140.5	126.4	126.4	111.2	2.60	1.23	0.64	156.30	0.81	127.2	1.14	1.478	2.00	0.88	102.56	1.23
C4_L6	140×70×10×3.5	8.68	7500	150	84.3	75.3	75.3	93.8	1.26	1.23	0.64	80.65	0.93	95.6	1.02	1.902	2.00	0.88	80.65	0.93
		8.68	7500	300	100.6	89.2	89.2	93.8	1.79	1.23	0.64	98.95	0.90	95.6	1.02	1.902	2.00	0.88	86.42	1.03
		8.68	7500	450	108.2	93.1	93.1	93.8	2.19	1.23	0.64	115.65	0.81	95.6	1.02	1.902	2.00	0.88	86.42	1.08
		8.68	7500	600	110.8	94.9	94.9	93.8	2.53	1.23	0.64	129.18	0.73	95.6	1.02	1.902	2.00	0.88	86.42	1.10
		8.68	7500	750	111.2	95.8	95.8	93.8	2.83	1.23	0.64	140.76	0.68	95.6	1.02	1.902	2.00	0.88	86.42	1.11

Column	Geometry			SFEA				DMS Design												
	$b_w \times b_f \times b_l \times t$	β_{FT}	L	f_y	$P_{u.FT}$	$P_{u.Fm}$	P_u	$f_{cr.FT}$	λ_{FT}	b	a	P_{nFT}	$\frac{P_u}{P_{nFT}}$	$f_{b.Fm}$	R_G	c	b	a	$P_{nFT\text{-}G}$	$\frac{P_u}{P_{nFT-G}}$
C5_L1	80×65×15×4.5	3.24	5300	150	120.0	133.2	120.0	129.5	1.08	0.90	0.56	110.85	1.08	186.0	1.44	0.899	1.09	0.61	110.85	1.08
		3.24	5300	300	146.4	186.0	146.4	129.5	1.52	0.90	0.56	138.56	1.06	186.0	1.44	0.899	1.09	0.61	138.18	1.06
		3.24	5300	450	159.6	201.6	159.6	129.5	1.86	0.90	0.56	173.02	0.92	186.0	1.44	0.899	1.09	0.61	166.07	0.96
		3.24	5300	600	169.2	208.8	169.2	129.5	2.15	0.90	0.56	202.56	0.84	186.0	1.44	0.899	1.09	0.61	189.20	0.89
		3.24	5300	750	178.8	212.4	178.8	129.5	2.41	0.90	0.56	228.90	0.78	186.0	1.44	0.899	1.09	0.61	209.34	0.85
C5_L2	80×65×15×4.5	3.24	5500	150	117.4	129.6	117.4	124.6	1.10	0.90	0.56	108.75	1.08	172.7	1.39	1.044	1.24	0.64	108.75	1.08
		3.24	5500	300	141.6	175.2	141.6	124.6	1.55	0.90	0.56	136.16	1.04	172.7	1.39	1.044	1.24	0.64	134.63	1.05
		3.24	5500	450	153.6	188.4	153.6	124.6	1.90	0.90	0.56	170.03	0.90	172.7	1.39	1.044	1.24	0.64	157.12	0.98
		3.24	5500	600	163.2	194.4	163.2	124.6	2.19	0.90	0.56	199.06	0.82	172.7	1.39	1.044	1.24	0.64	175.31	0.93
		3.24	5500	750	170.4	196.8	170.4	124.6	2.45	0.90	0.56	224.94	0.76	172.7	1.39	1.044	1.24	0.64	190.86	0.89
C5_L3	80×65×15×4.5	3.24	6000	150	110.2	118.1	110.2	113.7	1.15	0.90	0.56	103.63	1.06	145.1	1.28	1.25	1.44	0.70	103.63	1.06
		3.24	6000	300	129.6	151.2	129.6	113.7	1.62	0.90	0.56	130.64	0.99	145.1	1.28	1.25	1.44	0.70	125.15	1.04
		3.24	6000	450	139.2	160.8	139.2	113.7	1.99	0.90	0.56	163.14	0.85	145.1	1.28	1.25	1.44	0.70	140.08	0.99
		3.24	6000	600	146.4	164.4	146.4	113.7	2.30	0.90	0.56	190.98	0.77	145.1	1.28	1.25	1.44	0.70	151.74	0.96
		3.24	6000	750	152.4	166.8	152.4	113.7	2.57	0.90	0.56	215.82	0.71	145.1	1.28	1.25	1.44	0.70	161.45	0.94
C5_L4	80×65×15×4.5	3.24	6500	150	103.3	107.5	103.3	104.5	1.20	0.90	0.56	98.71	1.05	123.7	1.18	1.397	1.59	0.74	98.71	1.05
		3.24	6500	300	119.3	132.0	119.3	104.5	1.69	0.90	0.56	125.75	0.95	123.7	1.18	1.397	1.59	0.74	115.66	1.03
		3.24	6500	450	127.2	138.0	127.2	104.5	2.08	0.90	0.56	157.03	0.81	123.7	1.18	1.397	1.59	0.74	125.66	1.01
		3.24	6500	600	132.0	141.6	132.0	104.5	2.40	0.90	0.56	183.83	0.72	123.7	1.18	1.397	1.59	0.74	133.27	0.99
		3.24	6500	750	135.6	142.8	135.6	104.5	2.68	0.90	0.56	207.74	0.65	123.7	1.18	1.397	1.59	0.74	139.50	0.97
C5_L5	80×65×15×4.5	3.24	7000	150	97.1	97.3	97.1	96.5	1.25	0.90	0.56	93.91	1.03	106.6	1.10	1.578	1.77	0.80	93.91	1.03
		3.24	7000	300	110.2	115.2	110.2	96.5	1.76	0.90	0.56	121.30	0.91	106.6	1.10	1.578	1.77	0.80	105.43	1.04
		3.24	7000	450	115.8	120.0	115.8	96.5	2.16	0.90	0.56	151.48	0.76	106.6	1.10	1.578	1.77	0.80	110.41	1.05
		3.24	7000	600	119.3	122.4	119.3	96.5	2.49	0.90	0.56	177.33	0.67	106.6	1.10	1.578	1.77	0.80	114.08	1.05
		3.24	7000	750	121.2	123.6	121.2	96.5	2.79	0.90	0.56	200.39	0.60	106.6	1.10	1.578	1.77	0.80	117.02	1.04
C5_L6	80×65×15×4.5	3.24	7600	150	84.5	86.0	84.5	88.1	1.30	0.90	0.56	88.26	0.96	90.4	1.03	1.869	2.00	0.88	88.26	0.96
		3.24	7600	300	100.1	99.0	99.0	88.1	1.85	0.90	0.56	116.41	0.85	90.4	1.03	1.869	2.00	0.88	92.77	1.07
		3.24	7600	450	103.8	102.6	102.6	88.1	2.26	0.90	0.56	145.36	0.71	90.4	1.03	1.869	2.00	0.88	92.77	1.11
		3.24	7600	600	105.7	104.4	104.4	88.1	2.61	0.90	0.56	170.18	0.61	90.4	1.03	1.869	2.00	0.88	92.77	1.13
		3.24	7600	750	106.7	105.4	105.4	88.1	2.92	0.90	0.56	192.31	0.55	90.4	1.03	1.869	2.00	0.88	92.77	1.14
C6_L1	95×50×10×2	8.65	2700	150	53.5	56.7	53.5	227.7	0.81	1.23	0.64	48.96	1.09	398.6	1.75	0.71	1.23	0.64	48.96	1.09
		8.65	2700	300	80.7	100.9	80.7	227.7	1.15	1.23	0.64	74.32	1.09	398.6	1.75	0.71	1.23	0.64	74.32	1.09
		8.65	2700	450	90.8	127.0	90.8	227.7	1.41	1.23	0.64	84.61	1.07	398.6	1.75	0.71	1.23	0.64	84.61	1.07
		8.65	2700	600	97.2	138.7	97.2	227.7	1.62	1.23	0.64	91.31	1.06	398.6	1.75	0.71	1.23	0.64	91.31	1.06
		8.65	2700	750	103.0	144.1	103.0	227.7	1.81	1.23	0.64	99.51	1.03	398.6	1.75	0.71	1.23	0.64	99.51	1.03
C6_L2	95×50×10×2	8.65	3500	150	45.4	50.9	45.4	146.7	1.01	1.23	0.64	42.04	1.08	239.5	1.63	0.71	1.23	0.64	42.04	1.08
		8.65	3500	300	59.0	78.0	59.0	146.7	1.43	1.23	0.64	54.81	1.08	239.5	1.63	0.71	1.23	0.64	54.81	1.08
		8.65	3500	450	66.4	87.8	66.4	146.7	1.75	1.23	0.64	62.38	1.07	239.5	1.63	0.71	1.23	0.64	62.38	1.07
		8.65	3500	600	73.0	92.3	73.0	146.7	2.02	1.23	0.64	69.69	1.05	239.5	1.63	0.71	1.23	0.64	69.69	1.05
		8.65	3500	750	78.3	94.5	78.3	146.7	2.26	1.23	0.64	75.95	1.03	239.5	1.63	0.71	1.23	0.64	75.95	1.03
C6_L3	95×50×10×2	8.65	4500	150	35.8	41.2	35.8	99.2	1.23	1.23	0.64	34.25	1.05	145.3	1.46	0.795	1.31	0.66	34.25	1.05
		8.65	4500	300	44.6	53.2	44.6	99.2	1.74	1.23	0.64	41.95	1.06	145.3	1.46	0.795	1.31	0.66	41.43	1.08
		8.65	4500	450	50.9	56.7	50.9	99.2	2.13	1.23	0.64	49.04	1.04	145.3	1.46	0.795	1.31	0.66	47.61	1.07
		8.65	4500	600	55.2	58.2	55.2	99.2	2.46	1.23	0.64	54.80	1.01	145.3	1.46	0.795	1.31	0.66	52.55	1.05
		8.65	4500	750	57.7	59.0	57.7	99.2	2.75	1.23	0.64	59.72	0.97	145.3	1.46	0.795	1.31	0.66	56.74	1.02
C6_L4	95×50×10×2	8.65	5500	150	29.3	31.8	29.3	74.9	1.42	1.23	0.64	27.89	1.05	97.3	1.30	1.214	1.73	0.79	27.89	1.05
		8.65	5500	300	36.1	37.4	36.1	74.9	2.00	1.23	0.64	35.30	1.02	97.3	1.30	1.214	1.73	0.79	30.52	1.18
		8.65	5500	450	40.0	39.0	39.0	74.9	2.45	1.23	0.64	41.27	0.94	97.3	1.30	1.214	1.73	0.79	32.22	1.21
		8.65	5500	600	41.7	39.7	39.7	74.9	2.83	1.23	0.64	46.11	0.86	97.3	1.30	1.214	1.73	0.79	33.48	1.19
		8.65	5500	750	42.3	40.0	40.0	74.9	3.16	1.23	0.64	50.25	0.80	97.3	1.30	1.214	1.73	0.79	34.49	1.16
C6_L5	95×50×10×2	8.65	6500	150	24.8	24.5	24.5	60.7	1.57	1.23	0.64	23.75	1.03	69.7	1.15	1.468	1.99	0.87	22.92	1.07
		8.65	6500	300	29.5	27.5	27.5	60.7	2.22	1.23	0.64	31.02	0.89	69.7	1.15	1.468	1.99	0.87	23.02	1.19
		8.65	6500	450	31.2	28.3	28.3	60.7	2.72	1.23	0.64	36.27	0.78	69.7	1.15	1.468	1.99	0.87	23.08	1.23
		8.65	6500	600	31.6	28.7	28.7	60.7	3.14	1.23	0.64	40.52	0.71	69.7	1.15	1.468	1.99	0.87	23.13	1.24
		8.65	6500	750	31.6	28.8	28.8	60.7	3.52	1.23	0.64	44.16	0.65	69.7	1.15	1.468	1.99	0.87	23.16	1.25
C6_L6	95×50×10×2	8.65	7500	150	21.5	19.2	19.2	51.6	1.70	1.23	0.64	21.49	0.89	52.4	1.02	1.92	2.00	0.88	19.47	0.99
		8.65	7500	300	24.1	20.9	20.9	51.6	2.41	1.23	0.64	28.07	0.75	52.4	1.02	1.92	2.00	0.88	19.47	1.08
		8.65	7500	450	24.5	21.5	21.5	51.6	2.95	1.23	0.64	32.82	0.65	52.4	1.02	1.92	2.00	0.88	19.47	1.10
		8.65	7500	600	24.5	21.8	21.8	51.6	3.41	1.23	0.64	36.67	0.59	52.4	1.02	1.92	2.00	0.88	19.47	1.12
		8.65	7500	750	24.5	21.8	21.8	51.6	3.81	1.23	0.64	39.96	0.54	52.4	1.02	1.92	2.00	0.88	19.47	1.12

Column	Geometry			SFEA				DMS Design												
	$b_w \times b_f \times b_l \times t$	β_{FT}	L	f_y	$P_{u.FT}$	$P_{u.Fm}$	P_u	$f_{cr.FT}$	λ_{FT}	b	a	P_{nFT}	$\frac{P_u}{P_{nFT}}$	$f_{b.Fm}$	R_G	c	b	a	$P_{nFT\text{-}G}$	$\frac{P_u}{P_{nFT-G}}$
C7_L1	75×60×10×3.5	3.50	5200	150	77.6	86.9	77.6	109.7	1.17	0.92	0.57	72.78	1.07	155.4	1.42	0.961	1.17	0.63	72.78	1.07
		3.50	5200	300	92.9	114.4	92.9	109.7	1.65	0.92	0.57	91.98	1.01	155.4	1.42	0.961	1.17	0.63	89.76	1.03
		3.50	5200	450	101.5	122.1	101.5	109.7	2.03	0.92	0.57	114.50	0.89	155.4	1.42	0.961	1.17	0.63	106.19	0.96
		3.50	5200	600	109.2	125.6	109.2	109.7	2.34	0.92	0.57	133.75	0.82	155.4	1.42	0.961	1.17	0.63	119.63	0.91
		3.50	5200	750	114.4	127.3	114.4	109.7	2.61	0.92	0.57	150.88	0.76	155.4	1.42	0.961	1.17	0.63	131.23	0.87
C7_L2	75×60×10×3.5	3.50	5500	150	74.2	82.0	74.2	103.8	1.20	0.92	0.57	70.45	1.05	138.9	1.34	1.147	1.36	0.68	70.45	1.05
		3.50	5500	300	87.7	104.1	87.7	103.8	1.70	0.92	0.57	89.68	0.98	138.9	1.34	1.147	1.36	0.68	84.90	1.03
		3.50	5500	450	95.5	110.1	95.5	103.8	2.08	0.92	0.57	111.63	0.86	138.9	1.34	1.147	1.36	0.68	96.74	0.99
		3.50	5500	600	101.5	112.7	101.5	103.8	2.40	0.92	0.57	130.39	0.78	138.9	1.34	1.147	1.36	0.68	106.12	0.96
		3.50	5500	750	105.8	114.4	105.8	103.8	2.69	0.92	0.57	147.09	0.72	138.9	1.34	1.147	1.36	0.68	114.02	0.93
C7_L3	75×60×10×3.5	3.50	6000	150	69.7	73.6	69.7	95.2	1.26	0.92	0.57	66.71	1.05	116.8	1.23	1.324	1.53	0.73	66.71	1.05
		3.50	6000	300	80.7	89.4	80.7	95.2	1.78	0.92	0.57	86.18	0.94	116.8	1.23	1.324	1.53	0.73	77.71	1.04
		3.50	6000	450	86.9	93.7	86.9	95.2	2.17	0.92	0.57	107.28	0.81	116.8	1.23	1.324	1.53	0.73	85.40	1.02
		3.50	6000	600	91.2	95.5	91.2	95.2	2.51	0.92	0.57	125.31	0.73	116.8	1.23	1.324	1.53	0.73	91.32	1.00
		3.50	6000	750	93.7	96.3	93.7	95.2	2.81	0.92	0.57	141.36	0.66	116.8	1.23	1.324	1.53	0.73	96.19	0.97
C7_L4	75×60×10×3.5	3.50	6500	150	65.2	65.9	65.2	87.9	1.31	0.92	0.57	63.15	1.03	99.5	1.13	1.51	1.72	0.78	63.15	1.03
		3.50	6500	300	74.1	77.1	74.1	87.9	1.85	0.92	0.57	83.07	0.89	99.5	1.13	1.51	1.72	0.78	70.39	1.05
		3.50	6500	450	78.4	80.3	78.4	87.9	2.26	0.92	0.57	103.41	0.76	99.5	1.13	1.51	1.72	0.78	74.57	1.05
		3.50	6500	600	81.0	81.8	81.0	87.9	2.61	0.92	0.57	120.79	0.67	99.5	1.13	1.51	1.72	0.78	77.68	1.04
		3.50	6500	750	82.5	82.6	82.5	87.9	2.92	0.92	0.57	136.26	0.61	99.5	1.13	1.51	1.72	0.78	80.19	1.03
C7_L5	75×60×10×3.5	3.50	6800	150	62.7	61.5	61.5	84.0	1.34	0.92	0.57	61.09	1.01	90.1	1.07	1.68	1.89	0.84	61.09	1.01
		3.50	6800	300	70.4	71.0	70.4	84.0	1.89	0.92	0.57	81.36	0.87	90.1	1.07	1.68	1.89	0.84	65.02	1.08
		3.50	6800	450	73.9	73.7	73.7	84.0	2.31	0.92	0.57	101.27	0.73	90.1	1.07	1.68	1.89	0.84	66.49	1.11
		3.50	6800	600	75.7	74.9	74.9	84.0	2.67	0.92	0.57	118.30	0.63	90.1	1.07	1.68	1.89	0.84	67.55	1.11
		3.50	6800	750	76.6	75.7	75.7	84.0	2.99	0.92	0.57	133.45	0.57	90.1	1.07	1.68	1.89	0.84	68.39	1.11
C7_L6	75×60×10×3.5	3.50	7200	150	59.5	56.2	56.2	79.2	1.38	0.92	0.57	58.39	0.96	81.1	1.02	1.879	2.00	0.88	58.39	0.96
		3.50	7200	300	65.9	63.8	63.8	79.2	1.95	0.92	0.57	79.19	0.81	81.1	1.02	1.879	2.00	0.88	59.77	1.07
		3.50	7200	450	68.2	66.0	66.0	79.2	2.38	0.92	0.57	98.57	0.67	81.1	1.02	1.879	2.00	0.88	59.77	1.11
		3.50	7200	600	69.2	67.1	67.1	79.2	2.75	0.92	0.57	115.14	0.58	81.1	1.02	1.879	2.00	0.88	59.77	1.12
		3.50	7200	750	69.6	67.7	67.7	79.2	3.08	0.92	0.57	129.89	0.52	81.1	1.02	1.879	2.00	0.88	59.77	1.13
C8_L1	80×45×11×2	7.38	2000	150	51.4	52.5	51.4	319.7	0.68	1.15	0.62	47.33	1.09	626.2	1.96	0.71	1.15	0.62	47.33	1.09
		7.38	2000	300	87.7	99.5	87.7	319.7	0.97	1.15	0.62	77.78	1.13	626.2	1.96	0.71	1.15	0.62	77.78	1.13
		7.38	2000	450	104.4	138.5	104.4	319.7	1.19	1.15	0.62	95.87	1.09	626.2	1.96	0.71	1.15	0.62	95.87	1.09
		7.38	2000	600	112.0	163.5	112.0	319.7	1.37	1.15	0.62	105.04	1.07	626.2	1.96	0.71	1.15	0.62	105.04	1.07
		7.38	2000	750	117.2	176.1	117.2	319.7	1.53	1.15	0.62	109.65	1.07	626.2	1.96	0.71	1.15	0.62	109.65	1.07
C8_L2	80×45×11×2	7.38	2500	150	47.4	49.9	47.4	216.9	0.83	1.15	0.62	43.12	1.10	397.1	1.83	0.71	1.15	0.62	43.12	1.10
		7.38	2500	300	69.9	90.7	69.9	216.9	1.18	1.15	0.62	64.57	1.08	397.1	1.83	0.71	1.15	0.62	64.57	1.08
		7.38	2500	450	78.4	115.2	78.4	216.9	1.44	1.15	0.62	72.51	1.08	397.1	1.83	0.71	1.15	0.62	72.51	1.08
		7.38	2500	600	84.3	127.2	84.3	216.9	1.66	1.15	0.62	79.77	1.06	397.1	1.83	0.71	1.15	0.62	79.77	1.06
		7.38	2500	750	89.8	133.2	89.8	216.9	1.86	1.15	0.62	87.68	1.02	397.1	1.83	0.71	1.15	0.62	87.68	1.02
C8_L3	80×45×11×2	7.38	3500	150	37.4	42.1	37.4	126.1	1.09	1.15	0.62	35.01	1.07	204.1	1.62	0.71	1.15	0.62	35.01	1.07
		7.38	3500	300	46.9	62.8	46.9	126.1	1.54	1.15	0.62	43.51	1.08	204.1	1.62	0.71	1.15	0.62	43.51	1.08
		7.38	3500	450	53.1	69.1	53.1	126.1	1.89	1.15	0.62	51.66	1.03	204.1	1.62	0.71	1.15	0.62	51.66	1.03
		7.38	3500	600	58.5	71.8	58.5	126.1	2.18	1.15	0.62	58.35	1.00	204.1	1.62	0.71	1.15	0.62	58.35	1.00
		7.38	3500	750	62.7	73.2	62.7	126.1	2.44	1.15	0.62	64.13	0.98	204.1	1.62	0.71	1.15	0.62	64.13	0.98
C8_L4	80×45×11×2	7.38	4500	150	29.3	33.8	29.3	88.2	1.30	1.15	0.62	28.27	1.04	123.6	1.40	1.00	1.45	0.70	28.27	1.04
		7.38	4500	300	35.9	41.6	35.9	88.2	1.84	1.15	0.62	35.40	1.01	123.6	1.40	1.00	1.45	0.70	33.32	1.08
		7.38	4500	450	40.4	43.8	40.4	88.2	2.26	1.15	0.62	42.04	0.96	123.6	1.40	1.00	1.45	0.70	37.27	1.09
		7.38	4500	600	43.3	44.8	43.3	88.2	2.61	1.15	0.62	47.48	0.91	123.6	1.40	1.00	1.45	0.70	40.35	1.07
		7.38	4500	750	45.0	45.3	45.0	88.2	2.92	1.15	0.62	52.19	0.86	123.6	1.40	1.00	1.45	0.70	42.92	1.05
C8_L5	80×45×11×2	7.38	5500	150	24.1	25.2	24.1	68.6	1.48	1.15	0.62	23.07	1.05	87.8	1.28	1.244	1.69	0.77	23.07	1.05
		7.38	5500	300	28.8	28.9	28.8	68.6	2.09	1.15	0.62	30.63	0.94	87.8	1.28	1.244	1.69	0.77	25.65	1.12
		7.38	5500	450	31.1	29.9	29.9	68.6	2.56	1.15	0.62	36.37	0.82	87.8	1.28	1.244	1.69	0.77	27.33	1.10
		7.38	5500	600	32.0	30.4	30.4	68.6	2.96	1.15	0.62	41.08	0.74	87.8	1.28	1.244	1.69	0.77	28.59	1.06
		7.38	5500	750	32.3	30.6	30.6	68.6	3.31	1.15	0.62	45.15	0.68	87.8	1.28	1.244	1.69	0.77	29.61	1.04
C8_L6	80×45×11×2	7.38	6500	150	20.5	19.2	19.2	56.8	1.63	1.15	0.62	20.48	0.94	59.3	1.04	1.79	2.00	0.88	19.14	1.00
		7.38	6500	300	23.1	21.1	21.1	56.8	2.30	1.15	0.62	27.47	0.77	59.3	1.04	1.79	2.00	0.88	19.14	1.10
		7.38	6500	450	23.8	21.7	21.7	56.8	2.81	1.15	0.62	32.62	0.66	59.3	1.04	1.79	2.00	0.88	19.14	1.13
		7.38	6500	600	23.9	21.9	21.9	56.8	3.25	1.15	0.62	36.85	0.60	59.3	1.04	1.79	2.00	0.88	19.14	1.15
		7.38	6500	750	23.9	22.1	22.1	56.8	3.63	1.15	0.62	40.50	0.55	59.3	1.04	1.79	2.00	0.88	19.14	1.15